ELSEVIER

Contents lists available at ScienceDirect

Quaternary Science Advances

journal homepage: www.sciencedirect.com/journal/quaternary-science-advances





Late Pleistocene glaciation in the southernmost Sangre de Cristo Mountains, New Mexico – Chronology and paleoclimate

Eric M. Leonard ^{a,*}, Benjamin J.C. Laabs ^b, Alexander Robertson ^a, Mitchell A. Plummer ^c, Daniel E. Ibarra ^d, Marc W. Caffee ^e

- ^a Department of Geology, Colorado College, Colorado Springs, CO, 80903, USA
- ^b Department of Earth, Environmental, and Geospatial Sciences, North Dakota State University, Fargo, ND, 58108-6050, USA
- ^c Idaho National Laboratory, P.O. Box 1625, Idaho Falls, ID, 83415-2107, USA
- d Department of Earth, Environmental and Planetary Science, and the Institute at Brown for Environment and Society, Brown University, Providence, RI, 02912, USA
- ^e Department of Physics and Astronomy and Department of Earth, Atmospheric, and Planetary Science, Purdue University, 525 Northwestern Ave, West Lafayette, IN, 47907-2036. USA

ARTICLE INFO

Keywords: Last glacial maximum Paleoclimate Cosmogenic surface-exposure dating Glacier modelling New Mexico Sangre de Cristo Mountains

ABSTRACT

Surface-exposure dating of moraine boulders and numerical paleoglacier modeling yield the first numerical ages for the local Last Glacial Maximum (LGM) in the state of New Mexico and the southernmost Rocky Mountains, and the first glacier-based paleoclimate estimates for that region. Analysis of cosmogenic ¹⁰Be in samples from ten moraine boulders indicates that glaciers in the Winsor Creek drainage in the southern Sangre de Cristo Mountains occupied their LGM positions until \sim 21.2 \pm 2.0 ka, and likely remained near those positions until about 18.3 \pm 1.3 ka. Application of a coupled energy/mass balance and ice-flow model to the reconstructed paleoglaciers indicates that temperature depressions of $8.6-9.0~^{\circ}\text{C}$ from present temperatures would have been necessary to sustain glaciers in the drainage at their last glacial maximum extents, assuming precipitation amounts and seasonality were no different from modern. Model uncertainly in these estimates is approximately ±1.5 °C. Combining glacier-model output with climate-model output interpolated to the study region suggests that the LGM glaciers in the drainage were likely sustained by a temperature depression of ~8 °C from modern conditions, coupled with an increase of \sim 10–25% in precipitation, at least during the fall-through-spring seasons. Such an increase in accumulation season precipitation is consistent with previous suggestions of enhancement of Pacific-sourced cyclonic precipitation due to southward displacement of the LGM mean winter storm track across the western United States and/or of increased intensity and penetration of Pacific atmospheric rivers into the continent at the LGM.

1. Introduction

Proxy records of environmental change during the last glaciation provide essential data for understanding how the climate system has operated in the past, and by extension, how it may be expected to operate in the future. Preserved records of changes in geomorphic, geochemical, and biological systems in the western United States provide evidence of significant spatial and temporal variability in late Pleistocene and Holocene climate change across the region. For example, nearly all available proxy records indicate that during the global Last Glacial Maximum (LGM – \sim 26.5–19 ka – Clark et al., 2009) significantly drier-than-present conditions were prevalent in the

northwestern U.S. and wetter-than-present conditions prevalent in the southwestern U.S. (Thompson et al., 1993; Oster et al., 2015, 2020; Ibarra et al., 2018). Proxy data also suggest greater LGM temperature depression relative to the present in the north compared to the south (Thompson et al., 1993). Most climate-modeling studies indicate similar climate patterns in the western U.S. during the LGM (e.g. COHMAP Members, 1988; Thompson et al., 1993; Lorenz et al., 2016; PMIP3 (https://pmip3.lsce.ipsl.fr [last accessed 2022-11-8]); Morrill et al., 2018; Osman et al., 2021). The nature, magnitude, spatial patterns and timing of climate change during the subsequent deglaciation are complex and remain a topic of ongoing research (Lora et al., 2016; Hudson et al., 2019; Lora and Ibarra, 2019; Palacios et al., 2020).

E-mail address: eleonard@coloradocollege.edu (E.M. Leonard).

https://doi.org/10.1016/j.qsa.2023.100070

 $^{^{\}ast}$ Corresponding author.

In the Rocky Mountains of the western United States the deposits of alpine glaciers are key proxy records of the LGM. In recent years the application of terrestrial cosmogenic nuclide (TCN) surface-exposure dating methods has led to significant improvement of our understanding of the timing, and the variability of timing, of local last glacial maxima and the subsequent deglaciation in the Rocky Mountains (Laabs et al., 2020). This work has focused almost exclusively on the central portions of the Rocky Mountains, in Colorado, Utah, Wyoming, and southernmost Montana (Fig. 1 insert). Work on extracting detailed climate information from paleoglaciers using numerical glacier models has similarly focused on the central portions of the Rocky Mountains (Laabs et al., 2006; Refsnider et al., 2008; Dühnforth and Anderson, 2011; Birkel et al., 2012; Schweinsberg et al., 2016; Leonard et al., 2017a; Brugger, 2010; Brugger et al., 2018, 2019, 2021; Quirk et al., 2018, 2020). Much less work has been done either further north in Montana or to the south in New Mexico. Recent work by Quirk et al. (2022) has provided a suite of TCN ages for the LGM and initial deglaciation, coupled with numerical-model results, in northern Rocky Mountains in western Montana. Glaciation in the southernmost portion of the Rocky Mountains, however, remains poorly investigated from both a chronological and a paleoclimate perspective. Modern climate in the southernmost Rocky Mountains region differs somewhat from

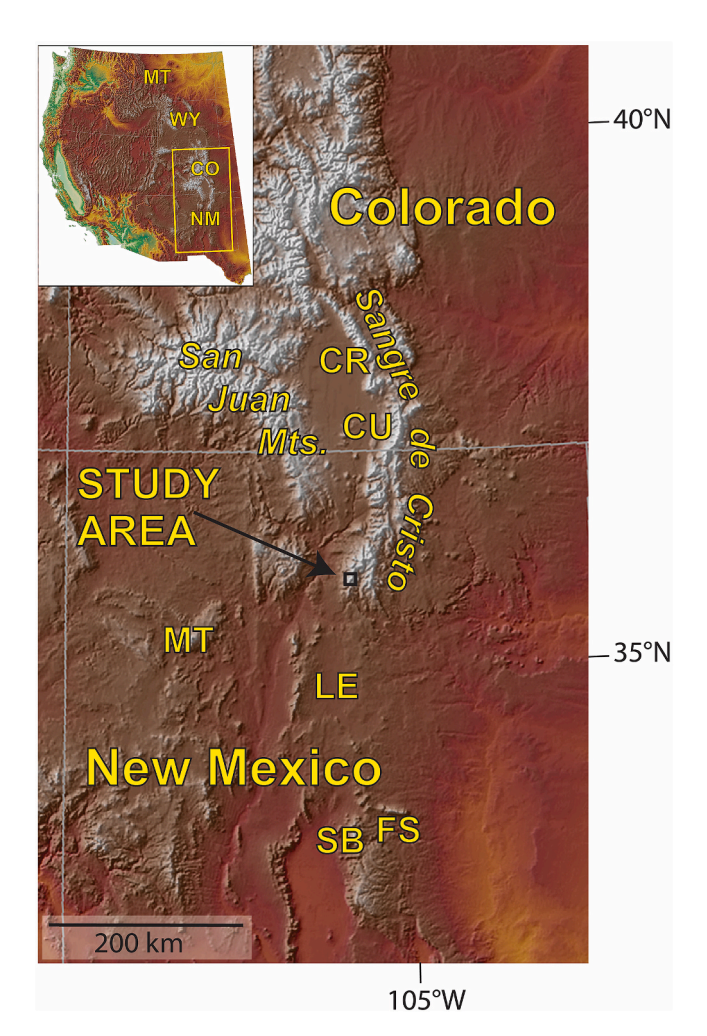


Fig. 1. Locality map of New Mexico and Colorado, indicating Winsor drainage study area and locations of other studies mentioned in text. CR = Crestone Peaks section of the northern Sangre de Cristo; CU = Culebra Peak section of the middle Sangre de Cristo; MT = Mount Taylor; LE = Pleistocene Lake Estancia; FS = Fort Stanton Cave; SB = Sierra Blanca. Inset map of the western United States shows location of main map and identifies Rocky Mountain states. MT = Montana; WY = Wyoming, CO = Colorado; NM = New Mexico.

climate further north, principally in the greater importance of convective summer monsoonal precipitation and relatively lesser importance of winter Pacific Ocean sourced cyclonic precipitation (Sheppard et al., 2002). A fuller understanding of the climatic conditions that led to LGM glaciation in this region may shed light on broader questions of late Pleistocene climate change in the western United States.

The state of New Mexico encompasses both the southernmost U.S. Rocky Mountains and portions of the lower-altitude U.S. Southwest (Fig. 1). While considerable work has been done there on low-altitude proxies for LGM climate, including lake-level, speleothem, and paleoecological studies (e.g. Antevs, 1954; Van Devender et al., 1984; Asmerom et al., 2010, 2017; Menking et al., 2018), much less work has been done in the more mountainous areas, and no numerically dated LGM glacial chronologies are currently available. This study examines the chronology and paleoclimate of the local LGM and subsequent deglaciation in the Winsor Creek drainage of the New Mexico Sangre de Cristo Mountains, the southernmost portion of the U.S. Rocky Mountains. We present the first numerical ages for LGM glaciers in the southernmost Rocky Mountains, coupled with previously published deglaciation ages for the same glacier system (Marcott et al., 2019), and an assessment of local LGM climate based on numerical glacier modeling.

2. Previous work

2.1. The last glaciation in New Mexico

The study of Late Pleistocene climate in New Mexico has focused primarily on the non-glacial record as glaciers were confined to only a relatively small portion of the state. Here we review first the current knowledge of Late Pleistocene glaciation and then outline briefly the non-glacial records.

2.1.1. Glacial records

Extensive Late Pleistocene glaciation in the southernmost Rocky Mountains was limited to the Sangre de Cristo Mountains and possibly the southern San Juan Mountains, both in the northern portion of New Mexico (Fig. 1) – with small valley glaciers in the former range as far south as ~35°45′ N. In the Sierra Blanca massif further south (~33°23′ N) (Fig. 1), Smith and Ray (1941) identified glacial deposits in a single valley and later workers (Richmond, 1963, 1964; Shroba, 1977) subdivided those into deposits of the last two major Northern Hemisphere glaciations, corresponding to marine isotope stages (MIS) 2 and 6 (Pierce, 2003). Sierra Blanca is generally considered to be the site of the southernmost Pleistocene glaciation in the continental United States (Smith and Ray, 1941; Pierce, 2003). Meyer et al. (2014) suggested that Mt. Taylor (~35°14′ N) (Fig. 1) may also have been glaciated, possibly during the late Pleistocene, but ultimately found the evidence equivocal.

Ray (1940) described glacier features in numerous valleys in four areas of the New Mexico Sangre de Cristo Mountains, identifying multiple depositional units which were attributed to different stades of the last, or "Wisconsin", glaciation. Richmond (1964) revisited some of the areas described by Ray, reinterpreting the deposits as products of two or three glaciations. Surprisingly little work has been done in the range since this early work. Shroba (1977) remapped glacial deposits originally mapped by Ray (1940) in the Nambe Creek drainage, a few kilometers southwest of our study area (Fig. 2), assigning them to the last two glaciations, and Jacobsen et al. (2010) did initial numerical modeling of LGM glaciers in that drainage. Recent work has been focused principally on the Winsor Creek drainage (Wesling, 1987, 1988; Armour et al., 2002; Jiménez-Marino et al., 2008; Marcott et al., 2019), the site of the current study. This work is described in section 3.1 below.

2.1.2. Non-glacial records

Evidence for late Quaternary climate change at lower-altitude sites in New Mexico has been the subject of considerable study since the middle

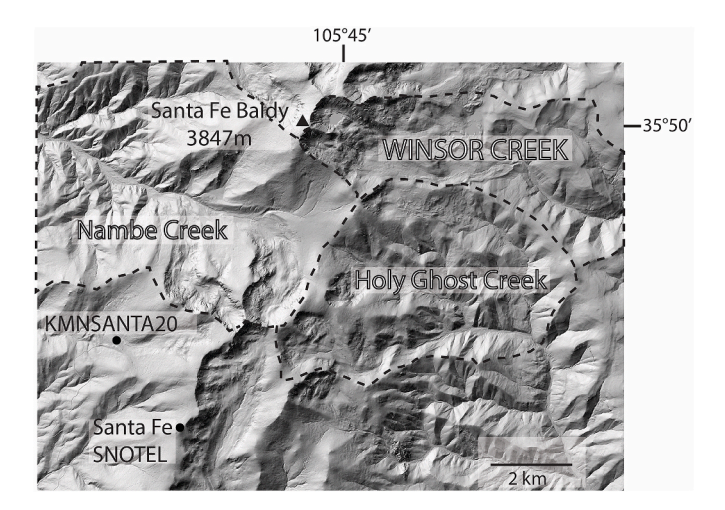


Fig. 2. –Digital terrain model showing upper Winsor Creek drainage and nearby glaciated drainages to the south and west. Filled circles indicate the approximate locations of the Santa Fe SNOTEL station and the personal weather station (KMNSANTA20) at Santa Fe ski area.

of the 20th century (e.g.; Antevs, 1935, 1954; Powers, 1939; Leopold, 1951). This work initially focused principally on changing "pluvial" lake levels and their paleoclimatic interpretation (e.g. – Antevs, 1935, 1954; Leopold, 1951; Brakenridge, 1978; Allen and Anderson, 2000; Menking et al., 2004; Allen, 2005) and on changing biota (Clisby and Sears, 1956; Wright et al., 1973; Van Devender et al., 1984; Hall et al., 2005). More recently, detailed records have been provided by isotopic analysis of well-dated cave speleothems (Polyak et al., 2012; Asmerom et al., 2010, 2017) and by a comparison of speleothem and lake records (Menking et al., 2018). Much of this work has focused on lake levels in the Estancia Basin and on speleothems from Fort Stanton Cave (Fig. 1). While a full review of this work is beyond the scope of the current paper, we return to the climatic implications of this non-glacial work in the region in the discussion section of this paper (section 6.3) to facilitate interpretation of our glacier-model results.

3. Study area

The current study focuses on the drainage of Winsor Creek, a tributary of the Pecos River, in the Santa Fe Range, the southernmost portion of the Sangre de Cristo Mountains (Figs. 1 and 2). The drainage

encompasses 18.8 km² of alpine and subalpine topography. Winsor Creek drains eastward for $\sim\!10$ km from the crest of the range at Santa Fe Baldy (3847 m) to its confluence with the Pecos River at $\sim\!2485$ m at Cowles, N.M. There is widespread erosional and deposition evidence of glaciation in the drainage above about 2900 m.

The main drainage heads in two deep glacial cirques below Santa Fe Baldy, the northern cirque occupied by Lake Katherine (Fig. 3). From the cirque floors (~3600 m) the drainage drops steeply to a broad midvalley bench at about 3100 m which marks the entry of a more northerly tributary valley draining a lower and less well-developed cirque. A complex of glacial deposits and associated modern lakes and bogs located on the mid-valley bench has been a focus of previous studies as well as much of the current study. East of the bench the drainage again drops steeply, through a latero-terminal moraine complex towards its confluence with the Pecos River. There are currently no glaciers or mapped permanent snowfields in the Winsor Creek drainage. A survey of New Mexico rock glaciers (Kinworthy, 2016) did not identify any in the drainage.

To some degree the morphology of the Winsor drainage basin reflects the underlying bedrock geology, with the topographic break downstream from the mid-valley bench at $\sim\!3100$ m corresponding to the Pecos-Picuris Fault. This fault separates primarily Pennsylvanian carbonate and siliciclastic sedimentary rocks to east, which underly lower part of basin, from Proterozoic granitic rocks and gneisses to the west, the latter underlying the higher parts of the basin and the range divide (Moench et al., 1988).

No meteorological data are currently collected within the Winsor Creek drainage. However, data are collected at several nearby high-altitude sites, notably the Santa Fe SNOTEL ($\underline{\text{snow}}$ telemetry) station at 3488 m about 10 km southwest of the study area (Fig. 2), which has operated continuously since 1996. Other nearby high-altitude data sources include the Wesner Springs SNOTEL (3389 m, \sim 17 km ESE, operated since 1988), and personal weather station KMNSANTA20 at Santa Fe ski area (3185 m, \sim 7 km WSW, operated since 2008 – Fig. 2). Lower-altitude data are available from the Elk Cabin SNOTEL (2502 m, \sim 16 km SSW, operated since 1996). Conditions at the Santa Fe and Wesner Springs SNOTELs and at the Santa Fe ski area are probably broadly representative of conditions in upper portions of the Winsor drainage, those at Elk Cabin SNOTEL of the lowest portions of the Winsor drainage.

Climate in the region is continental with large diurnal and seasonal temperature fluctuation and relatively low annual precipitation, but with strong influence of the North American (or "Southwest") summer monsoon (Sheppard et al., 2002). Mean annual precipitation generally

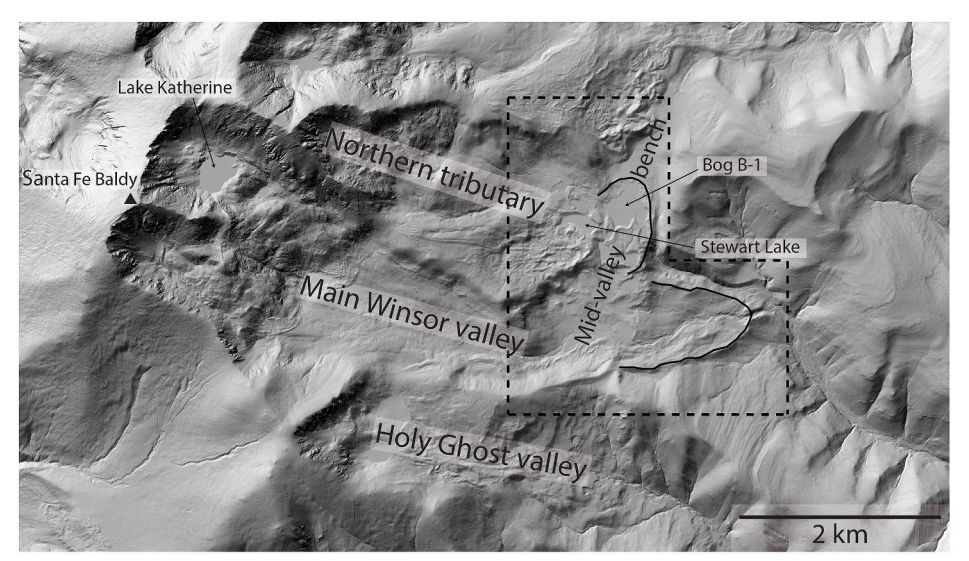


Fig. 3. Digital terrain model showing the main features of the glaciated portions of the Winsor Creek drainage and North Fork of the Holy Ghost Creek drainage. Outermost well-preserved moraines in the Winsor drainage are indicated by solid lines. Lake Katherine is the site of previously reported exposure ages (Marcott et al., 2019). Bog B-1 is the site of sediment cores analyzed by Armour et al. (2002) and Jiménez-Moreno et al. (2008). Dashed outline indicates area of mapping shown in Fig. 6.

increases with altitude, from 58.4 ± 10.9 cm at Elk Cabin SNOTEL, to 83.3 ± 17.4 cm and 90.1 ± 19.1 cm at Santa Fe and Wesner Springs SNOTELs respectively (mean values for 1997–2020 water years, the interval of overlap of continuous records from the three sites). Peak precipitation at all three SNOTEL sites occurs during the monsoon months of July and August, with monsoon precipitation playing an even stronger role at lower than at higher altitudes (Fig. 4). These two months account for 25% and 28% of the annual total precipitation at Santa Fe and Wesner Springs SNOTELs respectively, and 33% of the annual total at Elk Springs SNOTEL.

Tree line in the Winsor drainage currently ranges from about $3475 \, \mathrm{m}$ to $3600 \, \mathrm{m}$ depending on topography and aspect, which corresponds approximately to the altitude of the cirque floors.

3.1. Glacial deposits and history of the Winsor drainage

Wesling (1987, 1988) mapped glacial and other Quaternary deposits in the cirques, the mid-valley bench, and the downvalley moraine complex of the Winsor valley, with mapped glacial features extending about 4 km downvalley from the cirques. Ages were assigned primarily on the basis of soil development and clast weathering. In the cirques Wesling assigned ages spanning from the latest Pleistocene/early Holocene for deposits, including those impounding Lake Katherine in the northern cirque, to the early Neoglacial (mid-Holocene) for the youngest mapped moraines, including that just upvalley from the lake. Wesling reported a minimum limiting age of 3570 \pm 145 14 C yr BP (calibrated to a 2 σ age range of 3470–4286 cal yr BP, using Stuiver et al., 2021) for the youngest moraine in the southern cirque. Downvalley, a "Pinedale" (Last Glacial Maximum) age was assigned to glacial features on the mid-valley bench and a "Bull Lake" (penultimate glaciation) age to moraine ridges further downvalley, the distal-most and oldest glacial features identified.

Armour et al. (2002) cored a bog ("Bog B-1") inside the outermost moraine complex on the mid-valley bench (Fig. 3). A basal radiocarbon age from the core indicated deglaciation before $12,120 \pm 95$ ¹⁴C yr BP (calibrated to a 2σ age range of 13,785–14,311 cal yr BP, using Stuiver et al., 2021), predating the Younger Dryas interval (~12,900–11,700 yr

- Rasmussen et al., 2006). Based on sedimentological and isotopic analysis and dating of core sediment they suggested upvalley glacier readvances during the Younger Dryas chron (three radiocarbon ages ranging from $10{,}190\pm60$ to $9765\pm55\,^{14}$ C yr BP [calibrated to a 2σ age ranges of 11,502-12,421 cal yr BP and 10,886-11,269 cal yr BP, using Stuiver et al., 2021]). Four subsequent periods of increased clastic sedimentation were evident in the cores at ~4900, 3700, 2800 and 120 ¹⁴C yr BP. Armour et al. (2002) associated the second of these clastic sediment spikes with the timing of upvalley cirque moraine deposition, based on the minimum age provided by Wesling (1987, 1988). As the other three pulses of clastic sedimentation were not clearly associated in time with glacial deposits, Armour et al. (2002) interpreted them as evidence of enhanced periglacial processes driven by late Holocene cooling episodes. The bog currently receives drainage from the northern tributary, rather than the main Winsor Creek, and so these events recorded in the core likely reflect primarily the conditions in the northern cirque.

Jiménez-Moreno et al. (2008) undertook additional analysis of the cores collected by Armour et al. (2002), examining pollen and magnetic susceptibility. Much of the focus of their work was on reconstructing a detailed Holocene record, although data from the oldest core sections vield information on the end of the deglaciation interval. The coldest conditions evident in the pollen record, indicated by low arboreal pollen suggesting lowered treeline, occurred in the basal section of the core at ~14 cal ka BP. Subsequent vegetation changes indicate warming and treeline rise during the interval between ~13.8 and 12.8 cal ka BP, followed by a subtle cooling and attendant treeline lowering between ~12.2-11.5 cal ka BP. Jiménez-Moreno et al. (2008) associated the initial warming with the North Atlantic Bølling-Allerød interval (~14, 700-12,900 yr - Rasmussen et al., 2006) and the subsequent subtle cooling with the Younger Dryas. They also suggested that relatively high sediment-accumulation rates evident in the cores between \sim 11,880 and \sim 11,300 cal yr BP might reflect increased sediment flux at the end of the Younger Dryas period. Jiménez-Moreno et al. (2008) also documented millennial- and centennial-scale changes in vegetation and sedimentation rate through the Holocene. As the current study is focused on only the late Pleistocene of the valley, this portion of the work of

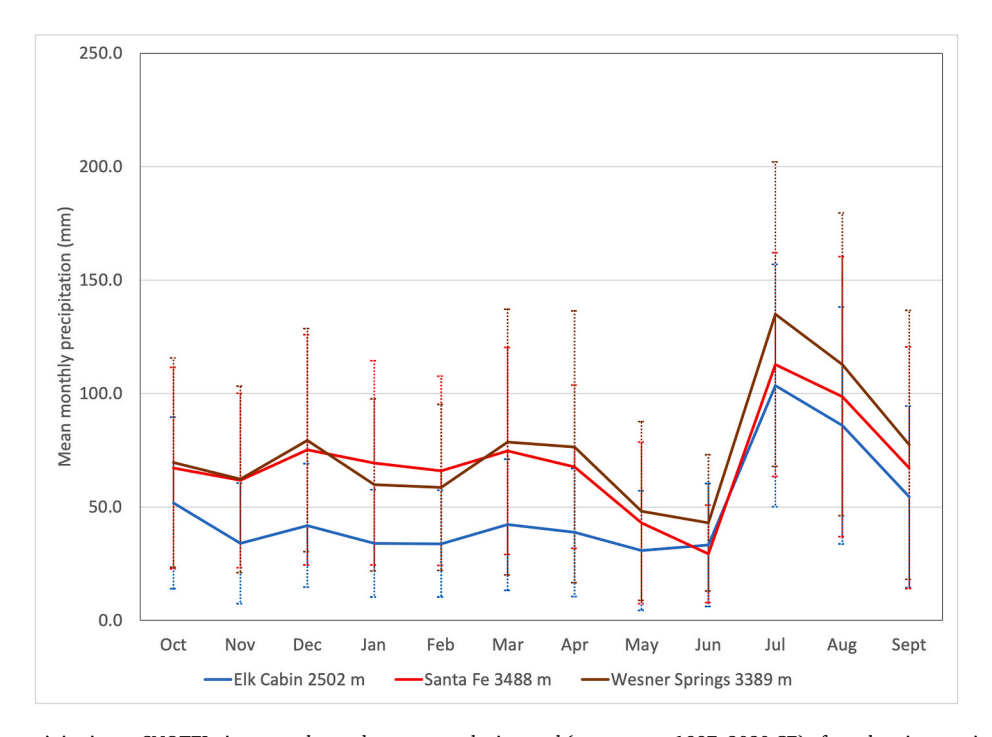


Fig. 4. – Mean monthly precipitation at SNOTEL sites near the study area over the interval (water years 1997–2020 CE) of overlapping continuous records. Error bars are 1σ standard deviation of monthly values at each site.

Jiménez-Moreno et al. (2008) is not discussed further.

Marcott et al. (2019) employed TCN surface-exposure dating to provide ages for glacial features in the Lake Katherine cirque. The apparent outer moraine in the cirque, identified by Wesling as "latest Pleistocene/early Holocene" yielded seven ^{10}Be exposure ages ranging from 14.7 ± 0.3 ka $(1\sigma$ internal uncertainty) to 15.5 ± 0.7 ka. An inner feature, but outside those mapped by Wesling as the late Holocene in age, yielded a broad range of ^{10}Be exposure ages (n=6) from 4.5 ± 0.1 ka to 18.0 ± 0.3 ka. Marcott et al. (2019) classified the two oldest ages and the single youngest age on this feature as "outliers". The remaining three ages from the feature overlapped with the ages on the outer feature, and Marcott et al. (2019) considered both to be features related to the same climate event – marked by an abandonment of glacier-related features at 15.1 ± 0.4 ka $(1\sigma$ standard deviation), indicating that the Lake Katherine cirque was mostly deglaciated well before the Younger Dryas.

Understanding of late Pleistocene glaciation and climate in the Winsor drainage remains incomplete. Wesling's (1987, 1988) work is the basis of our understanding of the pattern and chronology of glaciation, but this work was undertaken prior to the availability of LiDAR imagery, which has in many areas allowed major advances in geomorphic mapping, and nearly all of the age assignments were based on soil stratigraphy rather than numerical dating methods. The numerical ages that are now available are for only the uppermost portion of the drainage (Wesling, 1987, 1987; Marcott et al., 2019) and do not constrain the timing of the main glacial events represented by the downvalley moraines, or the pacing of the intervening deglaciation. While the paleoecological work of Amour et al. (2002) and Jiménez-Moreno et al. (2008) provides considerable insight into post-glacial (latest Pleistocene and Holocene) climate, these records do not extend back to the local last glacial maximum. In the current study we utilize a combination of mapping, TCN dating, and numerical modeling to investigate some of these remaining questions.

4. Methods

Methods utilized in this study included mapping of glacial and associated deposits, cosmogenic ¹⁰Be surface-exposure dating of moraine boulders, and numerical modeling of the glaciers that occupied the Winsor Creek drainage during the local last glacial maximum and the subsequent initial deglaciation. Mapping and ¹⁰Be sampling were focused on the mid-valley bench and the area immediately below, first because this is an area of complex topography, possibly reflecting the interactions around the time of the local last glacial maximum between ice from the main Winsor valley and that from the northern tributary valley, and possibly containing evidence of an earlier glaciation, and second because the timing of subsequent events in the upper portions of the valley has recently been constrained by the work of Marcott et al. (2019).

4.1. Mapping

Our mapping of glacial deposits was based on a combination of field reconnaissance and analysis of 1-m resolution LiDAR imagery sourced from the National Resource Conservation Service/U.S. Department of Agriculture. Our field mapping was limited to the area on and near the mid-valley bench, although we utilized LiDAR, in conjunction with numerical glacier modeling, to aid in understanding ice-flow patterns elsewhere in the drainage.

4.2. Cosmogenic ¹⁰Be surface exposure dating

We collected and analyzed samples from ten boulders from moraines on or immediately below the mid-valley bench – five from the outermost distinct moraines, five from moraines inside (or upvalley from) the outermost moraines. Samples were taken from large granitic or gneissic

boulders on low-slope (generally $<10^{\circ}$) sections of moraine crests, boulders that appeared to be well rooted in moraine material. Where possible, samples were taken from nearly horizontal, glacially polished, upper surfaces of boulders, at a height of 1 m or more above the neighboring moraine crest. In practice, however, most samples were taken from areas of single-grain (1–4 mm) relief on boulder surfaces, and for about half of the samples it was necessary to sample at just 60 cm to 1 m above the highest adjacent moraine surface.

Moraine boulder samples for cosmogenic ¹⁰Be exposure dating were prepared at SUNY Geneseo following methods of Laabs et al. (2013) with some modifications for beryllium extraction. Samples were reduced by crushing and milling, and the 250–500 μm grain size range was recovered by sieves. Magnetic grains were removed with a neodymium hand magnet and a Franz magnetic separator, and quartz grains were isolated using froth-flotation separation repeated dilute-acid treatments. Following methods of Kohl and Nishiizumi (1992), repeated etching in dilute hydrofluoric and nitric acids purified quartz, which was spiked with a commercially made ⁹Be carrier solution prior to dissolution. Procedural blanks were prepared using equal carrier mass to that added to samples and were used to correct ¹⁰Be/⁹Be of samples yielded by accelerator mass spectrometry (AMS) at the Purdue University Rare Isotope Measurement Laboratory (Sharma et al., 2000; Muzikar et al., 2003) by 6.00×10^{-15} , indicating that ¹⁰Be introduced by the carrier addition and sample preparation represents less than 1% of the in situ produced ¹⁰Be. Beryllium isotope ratios were measured using the AMS beryllium standard 07KNSTD (Nishiizumi et al., 2007).

Version 3.0 of the online exposure age calculators formerly known as CRONUS (Balco et al., 2008; http://hess.ess.washington.edu/math/[last accessed 2022-11-8]) were used to calculate ¹⁰Be exposure ages. Site-specific 10Be production rates were calculated with the Lifton-Sato-Dunai nuclide-dependent (LSDn; Lifton et al., 2014) scaling model and in situ ¹⁰Be data from the independently dated surface at the Promontory Point (PP) production-rate calibration site reported by Lifton et al. (2015). This calibration site was selected because it features continuously exposed surfaces following the Bonneville Flood at 18,350 \pm 300 cal yr BP, which are proximal in space and time to the study area and have been used in other recent reports of Pleistocene moraine chronologies in the Rocky Mountains (Licciardi and Pierce, 2018; Schweinsberg et al., 2020; Laabs et al., 2020; Tulenko et al., 2020; Quirk et al., 2022). In the text, tables, and figures in this paper all ages are reported on the basis of this preferred "PPLSDn" production rate and scaling combination. Sample ages determined using other production rate and scaling schemes are included in supplementary data. To ensure comparability, the ages of Marcott et al. (2019) from the Lake Katherine cirque were recalculated using the same calibration website and at the same time (April 19, 2022) as the ages reported in this study, using the same production rate and scaling schemes. The recalculated ages differed by no more than seven years from those originally reported by Marcott et al. (2019). We have made no weathering-related correction of exposure ages. We have also made no snow-shielding corrections. The height of boulder samples above the surrounding moraine likely minimized snow cover at the sample sites. Nonetheless, the potential for snow shielding does introduce the possibility that reported ages are slight underestimates.

4.3. Numerical glacier modeling

Paleoglaciers in and adjacent to the Winsor Creek drainage were modeled using the 2-d coupled energy/mass balance and flow model of Plummer and Phillips (2003) with a goal of understanding the changes from modern climate that would be necessary to sustain the mapped paleoglaciers. The energy/mass balance component of the model uses input modern climate values and energy balance parameters, ground-surface topography, and orbitally adjusted solar radiation parameters to generate a grid of annual snow accumulation and potential annual ice ablation across a model domain under the input climate. This

grid is then used as a distributed source term for the ice-flow component of the model, which utilizes input ice deformation and sliding parameters to "grow" a glacier to mass and flow equilibrium with the input climate. To simulate a possible paleoclimate, a set of instructions on how to alter climate from modern inputs is entered into the model, and appropriate orbitally constrained insolation parameters are substituted for modern parameters. The original model is discussed in detail in Plummer and Phillips (2003) and subsequent modifications to the model in Laabs et al. (2006) and Leonard et al. (2017a). A brief summary of the method follows, but readers are referred to those earlier papers for fuller discussion. Except as noted below, the methods utilized in this study are those presented in Leonard et al. (2017a).

The glacier-modeling domain encompassed 10.6 km², including the entirety of the glaciated portion of the Winsor drainage and the glaciated uppermost portion of the northern Holy Ghost Creek drainage to the south (Fig. 2). The latter area was included in the model domain as LiDAR evidence suggests that glacier ice at times overtopped the divide between the two drainages. All modeling was done at 20 m resolution on a digital elevation model derived from 10 m USGS DEMs. Model input parameters utilized in both the energy/mass balance component and the flow component are given in Table 1.

4.3.1. Energy/mass balance model

The energy/mass balance model calculates an annual net balance (annual snow accumulation in areas where accumulation exceeds ablation, and annual potential ice ablation in areas where potential ablation exceeds accumulation) for each 20-m pixel in the model domain. Calculations are made based on monthly values of mean temperature, temperature standard deviation, precipitation, relative humidity, wind speed, and cloud cover, as well as topographic shading. Snow accumulation is calculated from precipitation and temperature values, partitioning monthly precipitation between snow and rain depending on the fraction of the month that temperature is less than 2 °C, based on mean monthly temperature and the standard deviation of daily means temperatures for the month. Ablation, due to both sublimation and melt, is calculated from surface energy balance as described in detail by Plummer and Phillips (2003) and Laabs et al. (2006). Sources of modern climate data used as input to the model are detailed in Table 2.

Because there are no meteorological data collected within the Winsor drainage we utilized a combination of gridded climatology and observations from nearby SNOTEL and meteorological stations to characterize basin climate for model input. We utilized 15 arcsec (~400 m) grids of mean monthly temperature and precipitation (1971–2000 CE) produced by Climate Source by dynamic interpolation of PRISM (Parameter-elevation Regressions on Independent Slopes Model; htt p://www.prism.oregonstate.edu [last accessed 2022-11-8]; Daly et al.,

Table 1
Parameters used in glacier modeling.

Energy/mass-balance model parameters				
Snow albedo	0.8			
Ice albedo	0.4			
Snow/ice emissivity	0.99			
Basin emissivity	0.94			
Wind k ^a	$0.001 \; \mathrm{msec^{-1}}$			
Ground heat flux	0.1 Wm ⁻²			
Bulk-transfer coefficient	0.0015			
Flow-model parameters				
Deformation-law coefficient (A)	$7.5 \times 10^{-7} \text{ yr}^{-1} \text{kPa}^{-3}$			
Deformation-law exponent (n)	3			
Sliding-law coefficient (B)	$1.125 \times 10^{-2} \text{myr}^{-1} \text{kPa}^{-2}$			
Sliding-law exponent (m)	2			

^a Change in wind speed per meter of altitude.

2008) 30 arcsec grids. For each modeled 20-m grid cell, mean monthly temperature and precipitation were determined as a function of elevation, based on best fits of the 15 arcsec climatology to 15 arcsec grid altitudes in model domain. A linear best-fit was used to describe the temperature/altitude relationship. A second-order polynomial was used to describe the precipitation/altitude relationship as it provided a better fit to precipitation values in the highest- and lowest-altitude portions of the model domain.

Altitude is generally a very good predictor of temperature - with monthly linear regression r² values ranging from 0.968 to 0.996, averaging 0.986 for the year. Temperature lapse rates are generally fairly low, varying seasonally with lowest value of 0.42 °C/100 m in November and highest value of 0.62 °C/100 m in April. Equations for monthly temperature- and precipitation-verses-altitude relationships are tabulated in supplementary data (Table S-1). Precipitation is somewhat less well predicted by altitude, with the second-order relationship yielding monthly regression r² values ranging from 0.671 to 0.953, averaging 0.920 for the year. During the summer months of June through September, r² values average 0.822. For the other eight fallthrough-spring months of October through April the relationship is stronger, with r² averaging 0.942. Because summer precipitation is generally not a strong control on glacier mass balance, the relatively weak altitude vs. precipitation relationship during the summer is less concerning for our modeling than it would be during the fall-throughspring seasons. Data from the KMNSANTA20 personal weather station at Santa Fe ski area (Fig. 2 - https://www.wunderground.com/dashb oard/pws/KNMSANTA20 [last accessed 2022-11-8]) were used to approximate monthly mean of windspeed and relative humidity. Cloudiness (approximated as the proportion of days in a month with measurable precipitation) and variability of daily mean temperatures in the Winsor basin were approximated from records at the Santa Fe SNOTEL (Fig. 2 - https://wcc.sc.egov.usda.gov/nwcc/site? sitenum=922x [last accessed 2023-1-2]).

To model mass balance under past conditions, solar insolation values were varied to replicate those at the assumed time of the past ice extent. Other values necessary for input into the energy/mass balance model – including snow and ice albedo, snow and basin emissivity, bulk-transfer coefficient, wind-speed gradient with altitude, and ground heat flux – are our best estimates, based on literature values, and these values are listed in Table 1. Plummer and Phillips (2003) and Quirk et al. (2020) discussed many of these assumptions and their implications for model uncertainty, which is discussed in section 4.3.4 below. The model simulates redistribution of snow by avalanches on slopes exceeding 30°, but does not simulate redistribution of snow by wind.

4.3.2. Ice-flow model

The mass-balance model output grid, coupled with digitized topography of the model domain, provide input for the flow model. The latter is based on a finite-difference approach and combines the continuity equation for glacier mass flow with parameters relating internal deformation of ice and basal sliding of ice over the substrate to driving stresses generated by overlying ice thickness and ice-surface slope. Ice flow velocity is determined at each grid node by the equation:

$$u = u_d + u_s = \frac{2A}{n+2} \tau^n H + B \tau^m$$
 (Eq. 1)

where u is total velocity, u_d and u_s are velocities due to internal deformation and basal sliding respectively, A and B are flow- and sliding-law coefficients respectively, n and m are flow- and sliding-law exponents, taken as 3 and 2 respectively, and τ is the driving stress. Following Jarosch et al. (2013), we incorporate a flux-limiting scheme in the model. The specified ice-flow parameters are constant and uniform in the model domain.

We assume in all model simulations that basal ice temperature was at the pressure-melting point and that, consequently, basal sliding

Table 2Modern climate data used in glacier modeling.

Climate Parameter	Data source	Site	Latitude Longitude	Altitude (m)	Dates of record (CE)
Monthly mean temperature vs. altitude	PRISM 15-arc sec	Throughout basins	35 '48.75 to 35° 50.5' N 105° 42.5' to 105° 45.5' W	2945–3669	1971–2000
Monthly mean precipitation vs. altitude	PRISM 15-arc sec	Throughout basins	35 '48.75 to 35° 50.5' N 105° 42.5' to 105° 45.5' W	2945–3669	1971–2000
Monthly standard deviation of daily mean temperature, monthly mean percent of days with measurable precipitation ^a	SNOTEL (Snow Telemetry)	Santa Fe	35° 46′ N 105° 47′ W	3488	1997–2011
Monthly mean relative humidity, Monthly mean wind speed	PWS (Personal Weather Station)	Santa Fe ski area	35° 47′ N 105° 48′ W	3185	2008–2021

^a Used as approximation of monthly mean cloud cover.

occurred. In this study we use A and B coefficients of 7.5×10^{-7} $yr^{-1}kPa^{-3}$ and 1.125 $\stackrel{\cdot}{\times} 10^{-2} \; myr^{-1}kPa^{-2},$ slightly higher than those used in previous studies of late Pleistocene glaciers further north in the Rocky Mountains (Laabs et al., 2006; Refsnider et al., 2008; Leonard et al., 2017a; Quirk et al., 2018). We these higher parameters because they produce a better fit to the longitudinal profiles of the preserved moraines in the Winsor Creek drainage than do the parameters used in the earlier studies, with much less upvalley ice spillover of the lateral moraines when the modeled glacier is large enough to reach the terminal moraines. This apparent difference in flow characteristics may reflect differences in ice rheology or basal slip due to temperature or precipitation differences, possibly related to the amount of englacial or subglacial water present. The higher parameters generally produce a somewhat thinner, faster flowing, glacier, which requires slightly less temperature depression to reach it maximum extent than do the lower parameters used in Colorado and Utah. This difference, however, is quite small, with a reduction in necessary temperature depression of only ~0.0–0.3 °C over the range of temperature and precipitation changes modeled.

Flow modeling is based on a shallow-ice approximation approach (Hutter, 1983) – an assumption that longitudinal stresses can be neglected in modeling ice flow. While a full-Stokes approach, which considers longitudinal stresses, is likely more accurate for modeling flow velocities, it is much more computationally intensive, and comparison studies (Le Meur and Vincent, 2003; Leysinger Vieli and Gudmundsson, 2004) indicate that the two approaches yield similar ice extents and thicknesses, which are the focus of our modeling.

4.3.3. Paleoglacier fitting

Because our goal is to understand the changes from modern climate that could have sustained local glaciers at their LGM extents, simulations were run sequentially, altering input climate until the modeled glaciers were in mass-balance and flow equilibrium at their mapped LGM extents. In addition to providing information on paleoclimate, the modeling facilitated reconstruction of ice-flow characteristics at the LGM which aided our interpretation of landform genesis.

Models were run iteratively as the glacier thickens, to simulate the climate on its top surface. There are, of course, an infinite number of possible combinations of climate variables that could produce a glacier in mass-balance equilibrium with a given geometry. The principal controls on glacier mass balance are temperature, particularly ablationseason temperature, and precipitation, particularly accumulationseason precipitation (Ohmura et al., 1992; Oerlemans, 2001). As such, multiple simulations of the model were run to find combinations of temperature and precipitation change from modern conditions that could have sustained the glaciers in the drainage in mass-balance equilibrium at their mapped local last glacial maximum extents. In all simulations an equal temperature depression was applied for all months of the year, and precipitation seasonality was generally not altered.

However, as discussed in section 6.2 below, some proxy data and climate models indicate that precipitation seasonality may have been different at the LGM, with a possible increase in winter precipitation and reduction of summer monsoon precipitation. As a sensitivity test, a small number of simulations were run reducing input precipitation during each of the three monsoon-influenced months (July, August, September) to the mean value for monthly precipitation during May and June, the dry months immediately preceding the monsoon (Fig. 4). Other changes in summer conditions which would likely accompany a suppression of the monsoon, including possible changes in temperature, cloudiness, wind, and relative humidity are very difficult to estimate and are not included in these simulations. Consequently, results of the suppressed-monsoon simulations should be regarded as a simplified demonstration of the influence of shifting precipitation seasonality.

It is worth emphasizing that the inference of climates from our modeling assumes that the glaciers were in mass-balance equilibrium at the time the dated moraines were deposited and that the position of a moraine represents that dictated by a mean climate over a relatively long interval of moraine deposition. Anderson et al. (2014) suggested that moraine position may represent short-term forcing by interannual weather variability in addition to forcing by longer-period mean climate, and consequently, that the use of the outermost moraine in an LGM terminal moraine complex to characterize mean LGM climate likely overestimates the magnitude of LGM temperature depression or precipitation enhancement relative to today. Recent modeling work on Colorado paleoglaciers of similar size and in similar climates to the main Winsor paleoglacier by Leonard et al. (2019, unpublished results) indicates, however, that the error in paleoclimate reconstruction introduced by interannual variability is small, likely much less than 0.5 °C. In a similar way, the use of monthly means and a one-month time step in the energy/mass balance model may mask shorter-term variability in climate forcing that might effect mass-balance results in a non-linear fashion. Such forcing likely causes an underestimation of ablation (Farinotti, 2017) and thus result in an underestimation of the magnitude of climate change from present necessary to sustain the paleoglaciers at the position of the outermost moraines.

4.3.4. Model validation and uncertainty

Because neither modern glaciers nor permanent snowfields are present in or nearby the study area, we are not able to test directly the skill of the model and the appropriateness of the input modern climate data set and physical parameters (albedo, emissivity, wind-speed gradient, bulk-transfer coefficient, ice-flow and sliding parameters, etc.) by comparison of simulated and observed modern glacier geometry. As an alternative approach, we use the model to simulate seasonal evolution of the snowpack at the nearby Santa Fe SNOTEL site (Fig. 2 – https://wcc.sc.egov.usda.gov/nwcc/site?sitenum=922 [last accessed 2023-1-2]). This approach comes with several caveats. First, it can be employed only for the portion of the year during which snow is on the ground, so it

provides a better assessment of model skill in simulating accumulation than in simulating ablation. Second, the comparison is imperfect because although the Santa Fe SNOTEL is the closest survey site to the model domain, it is not located within the domain for which the model was developed and applied. Finally, the time interval of the PRISM/ Climate Source climate output from which our model was developed (1971-2000 CE) only incompletely overlaps the intervals for which temperature and precipitation norms are available for the SNOTEL station. Fig. 5 compares our simulated seasonal snowpack evolution with the measured median snowpack at the Santa Fe SNOTEL for the 1981-2010 and 1991-2020 intervals, based on a combination of SNO-TEL measurements, begun in the water year 1997 and earlier snow course measurements made at the same site. The model simulated a monthly snowpack evolution quite similar to the observed snowpack over both intervals. Compared to interval (1981–2010 CE) with the most temporal overlap with model's climate input, the simulation slightly underestimates the end-of-month accumulation through the accumulation season, and slightly overestimates the persistence of snowpack at the initiation of the ablation season. While the comparison indicates that the model does reasonably well at simulating seasonal snowpack evolution it does not allow a quantitative assessment of model skill or an overall assessment of the uncertainty in model results for the reasons

Quirk et al. (2020) recently ran a series of sensitivity tests in application of the model to reconstructed LGM glaciers in the Wasatch Range of Utah. They concluded that a reasonable range of uncertainties and possible past changes in windiness, cloud cover, relative humidity, albedo, and bulk-transfer coefficient introduce a potential error of about $\pm 1.0~^{\circ}\text{C}$ in paleotemperature inferred from model assuming no change from modern precipitation, equivalent to a $\pm 30\%$ precipitation uncertainty for an assumed paleotemperature. Their sensitivity analysis, however, did not consider several other sources of uncertainty in application of the model to paleoglaciers, including uncertainties in flow and sliding parameters, as well as possible past changes in seasonality and altitudinal gradients of temperature and precipitation, and effects of interannual and sub-monthly climate variability. Consequently we estimate overall uncertainty at about $\pm 1.5~^{\circ}\text{C}$.

500 450 400 of snowpack (mm) 350 300 equivalent depth 250 200 150 Water 100 50 Feb 1 Jly 1 Oct 1 Nov 1 Dec 1 Jan 1 Mar 1 Apr 1 May 1 Jun 1 Aug 1 Sep 1 Date in water year

5. Results

5.1. Mapping of glacial features

Our detailed examination of glacial features was limited to areas on and near the Winsor drainage midvalley bench, focusing on features related to the maximum extent of ice during the last (and possibly the penultimate) glaciation and initial recession from that maximum stand (Fig. 6). As noted by Wesling (1987, 1988), ice extended downvalley from the southern portion of the bench to a terminus marked by a well-preserved latero-terminal moraine complex (Figs. 3 and 6). Due to a realignment of the access trail, we were unable to visit the outermost right-lateral moraine fragment mapped previously by Wesling (1987, 1988) as corresponding to the Bull Lake glaciation, so it is not included in Fig. 6. Inside this moraine fragment is a large continuous moraine, present on both sides of the valley ("A" in Fig. 6), which Wesling (1987, 1988) also considered to be of Bull Lake age. Immediately inside this large moraine are several small moraine crests also in the area mapped by Wesling as "Bull Lake till". Further upvalley another conspicuous moraine crest ("B" in Fig. 6) is partially inset into, and partially overrides, the right lateral portion of moraine A. Moraine B was mapped by Armour et al. (2002) as the outermost Pinedale moraine, and although it was not mapped as an individual feature by Wesling (1987, 1988), it is in the area mapped as "Pinedale till". Armour et al. (2002) mapped this moraine as continuous with the outermost moraines on the northern portion of the midvalley bench, but we were unable to trace it across the valley floor, either in the field or on LiDAR, to be certain of its relationship to the northern moraines. Several lower and less distinct moraine crests are present inside moraine B.

On the northern portion of the midvalley bench an arcuate set of moraine crests marks the outermost extent of ice ("C" in Fig. 6). Absence of crystalline erratics in the area of sedimentary bedrock immediately east of this moraine complex suggests strongly that these moraines mark the greatest ice extent at least of recent glaciations. Inside and south of the arcuate moraines is an area of complex topography, with multiple moraine crests and intervening lakes, bog, and wet meadow areas. The relative contribution of main valley ice and northern tributary valley ice to the moraine complex on the northern part of the bench is not clear either on the ground or in LiDAR imagery and, as noted above, we have

Fig. 5. - Comparison of simulated and observed seasonal snowpack evolution for Santa Fe SNOTEL site. Red triangles indicate end-of-month waterequivalent depth of snowpack simulated using the model developed for the Winsor drainage in this study, based on PRISM/Climate Source temperature and precipitation values for the interval 1971-2000 CE. Blue line indicates median daily snow water-equivalent depth at the Santa Fe SNOTEL site for the interval 1981-2010 CE, based on a combination of snow-course data before 1997 CE and SNOTEL measurements since 1997 CE. Brown line indicates median daily snowpack water-equivalent depth at the Santa Fe SNOTEL site for the interval 1991-2020 CE, again based on a combination of snow-course and SNOTEL measurements. (For interpretation of the references to colour in this figure legend, the reader is referred to the Web version of this article.)

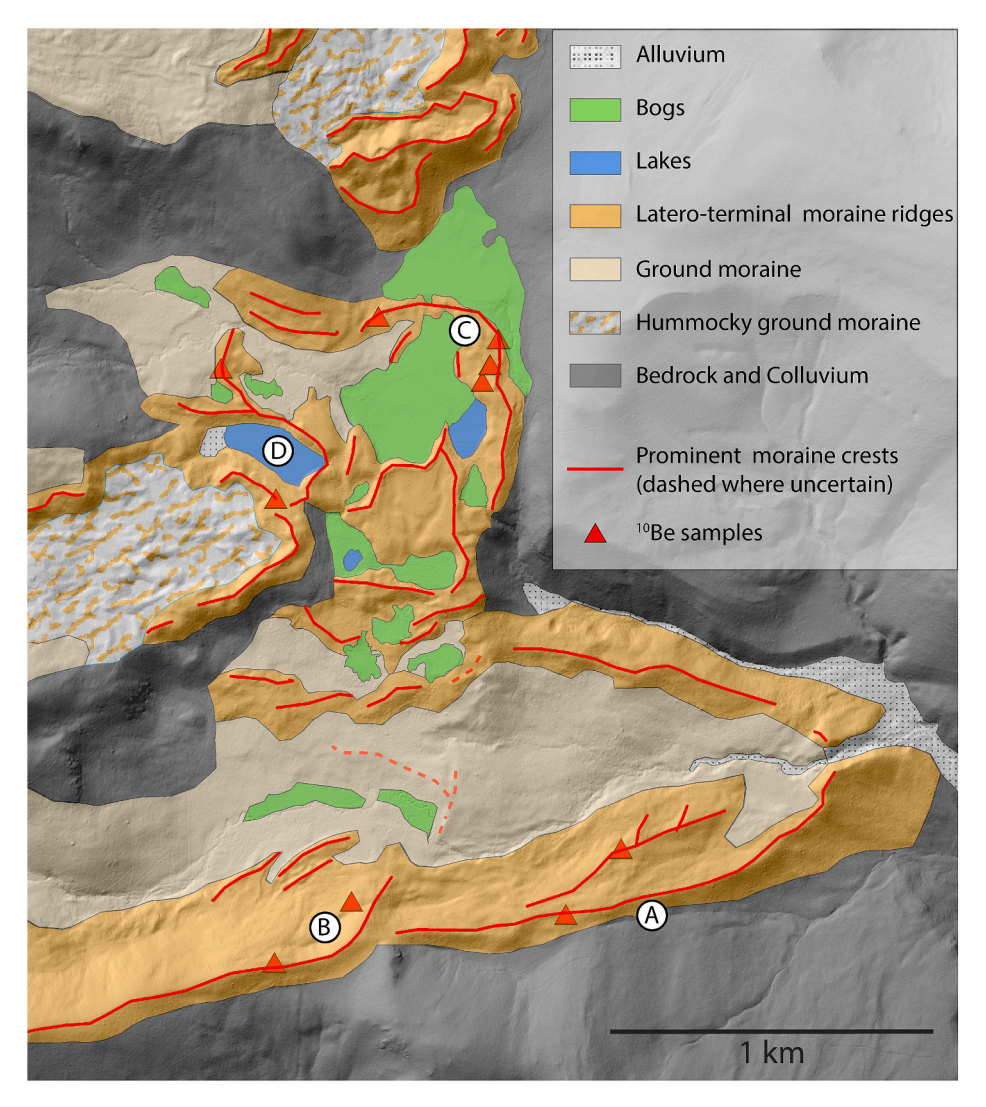


Fig. 6. Generalized geomorphological map of the lower glaciated portion of the Winsor Creek drainage. Areas mapped as moraine may contain some areas of glaciofluvial deposits. Circled letters indicate locations discussed in text section 5.1.

not been able to trace main-valley moraine B northward across the bench. In the northern tributary valley just west of the midvalley bench, multiple moraines are present impounding and neighboring Stewart Lake ("D" in Fig. 6). Because of uncertainty concerning the source of ice that produced the northern mid-valley bench moraine complex at "C", it is unclear whether the moraines slightly upvalley at Stewart Lake mark a maximum stand of the northern tributary glaciers or a pause or readvance during recession from the maximum stand. It is also unclear the degree to which the ice that deposited the moraines around Lake Stewart was sourced entirely in the northern tributary cirque and the extent to which upvalley spillover of ice from the main valley into the northern tributary valley may have contributed. A large area of apparent icestagnation topography (hummocky ground moraine) is present to the southwest of Stewart Lake, possibly the result of a shut-off of upvalley cross-divide flow from main valley glacier into the northern tributary valley as the former thinned during ice recession.

5.2. Surface exposure dating of moraine boulders

We obtained ¹⁰Be surface-exposure ages from ten moraine boulders in the Winsor drainage, five from the outermost moraine complexes and five from moraines further upvalley (Fig. 7, Tables 3, S-2, S-3, S-4). Separate isotope measurements were run on samples from two different surfaces of one of the boulders (WIN12-05 and WIN 12-05A). All

analyses, including those from segments of moraine previously identified as dating from the penultimate ("Bull Lake"-equivalent) glaciation (Wesling, 1987, 1988), yielded ages from the last ("Pinedale"-equivalent) glaciation. All but one of these age were in the 25-15 ka range.

Ages were obtained from five boulders on the outer moraine complexes. In the northern moraine complex ("C" in Figs. 6, Fig. 7) three boulders yielded ^{10}Be exposure ages ranging from 19.1 ± 0.5 ka to 24.0 \pm 0.9 ka, while a fourth boulder yielded an age of 39.5 ± 0.8 ka. A single boulder from the outermost moraine along the main valley ("A" in Figs. 6, Fig. 7) yielded a ^{10}Be age of 20.5 ± 0.5 ka.

Five ages were obtained on moraines upvalley from, or inside, the outer moraine complexes. A single boulder on the most downvalley of the small moraines immediately inside moraine A (Figs. 6 and 7) yielded $a^{10}Be$ age of 15.3 ± 0.6 ka. Two boulders on and just inside moraine B (Figs. 6 and 7) further upvalley yielded ages of 17.7 ± 0.4 ka and 19.8 ± 0.6 ka respectively. In the northern tributary valley, two boulders sampled on the moraines impounding Stewart Lake ("D" in Figs. 6, Fig. 7) yielded ages of 17.5 ± 0.5 ka and 22.7 ± 0.7 ka.

5.3. Numerical modeling of glaciers in the Winsor and Holy Ghost drainages

In the initial runs of the coupled energy/mass balance and flow

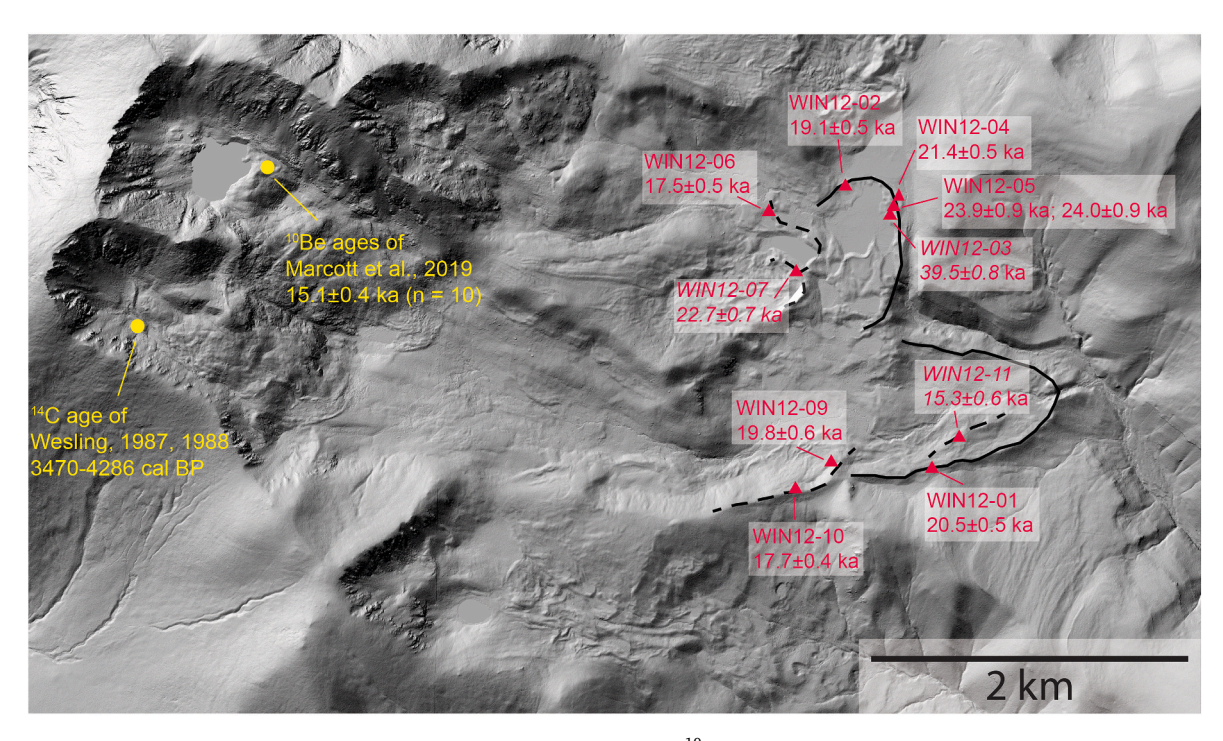


Fig. 7. Numerical ages of glacial deposits in the Winsor Creek drainage. Red triangles are 10 Be surface-exposure ages from moraines boulders sampled in this study. Ages are calculated using "PPLSDn" – the Promontory Point production local rate (Lifton et al., 2015) and Lifton-Sato-Dunai nuclide-dependent scaling (Lifton et al., 2014). Uncertainty values are reported as 1σ internal uncertainty. Separate age analyses were made for samples from two different surfaces of WIN12-05. Samples in italics are considered to be outliers, based on their ages and stratigraphic positions. Black lines indicate crest of moraines that were sampled for 10 Be ages. Yellow circles are ages published by previous workers in the upvalley cirques. 10 Be moraine boulder ages of Marcott et al. (2019) at Lake Katherine are recalculated using "PPLSDn" production rate and scaling and the reported uncertainty value is the 1σ standard deviation of the ten samples not considered outliers by those authors. The radiocarbon age of Wesling (1987, 1988) is a minimum age for a moraine in the southern cirque and is calibrated using Stuiver et al. (2021) and reported as a 95% certainty range. (For interpretation of the references to colour in this figure legend, the reader is referred to the Web version of this article.)

Table 3Cosmogenic 10Be sample information and exposure ages.

Sample ID	Latitude (°N)	Longitude (°E)	Elevation (m)	Thickness (cm)	Shielding	¹⁰ Be atoms/g	\pm atoms/	Age LSDn Promontory Point (ka)	Internal uncertainty (kyr)	External uncertainty (kyr)
WIN12- 01	35.82312	-105.7178	3072	1	0.9961	6.93E+05	1.61E+04	20.5	0.5	0.9
WIN12- 02	35.83372	-105.7232	3140	2.5	0.9935	6.61E+05	1.63E+04	19.1	0.5	0.9
WIN12- 03	35.83258	-105.7209	3131	1	0.998	1.45E+06	2.81E+04	39.5	0.8	1.7
WIN12- 04	35.83334	-105.7205	3129	2	0.9957	7.54E+05	1.62E+04	21.4	0.5	0.9
WIN12- 05	35.83288	-105.7207	3127	1	0.9844	8.56E+05	3.20E+04	24.0	0.9	1.3
WIN12- 05A	35.83288	-105.7207	3127	1	0.9884	8.56E+05	3.20E+04	23.9	0.9	1.3
WIN12- 06	35.83278	-105.7266	3153	2	0.9946	6.07E+05	1.57E+04	17.5	0.5	0.8
WIN12- 07	35.83047	-105.7254	3156	1	0.9941	8.27E+05	2.61E+04	22.7	0.7	1.1
WIN12- 09	35.82332	-105.7237	3097	2	0.9951	6.71E+05	2.09E+04	19.8	0.6	1.0
WIN12- 10	35.82212	-105.7253	3153	2	0.9904	6.11E+05	1.49E+04	17.7	0.4	0.8
WIN12- 11	35.82429	-105.7178	3027	2	0.9959	4.87E+05	2.00E+04	15.3	0.6	0.9

Note: all exposure age calculations assumed the standard air pressure model used in the Version 3 calculator (coded "std"), sample density of 2.7 g/cc, and zero surface erosion. All samples were measured against the AMS standard of Nishiizumi et al. (2007), coded "07KNSTD" in the Version 3 calculator.

model, we attempted to fit the simulated glaciers to the preserved outer moraines in the Winsor drainage by decreasing temperature uniformly throughout the year but making no change in monthly precipitation amounts. The model was run with solar-insolation parameters set to 21

ka, our best estimate of the time when the outer moraines were deposited. A $8.6-8.7\,^{\circ}$ C temperature depression provided the closest fit to the preserved moraines in the main valley, but under simulated the amount of ice necessary to reach the outer moraine complex on the northern

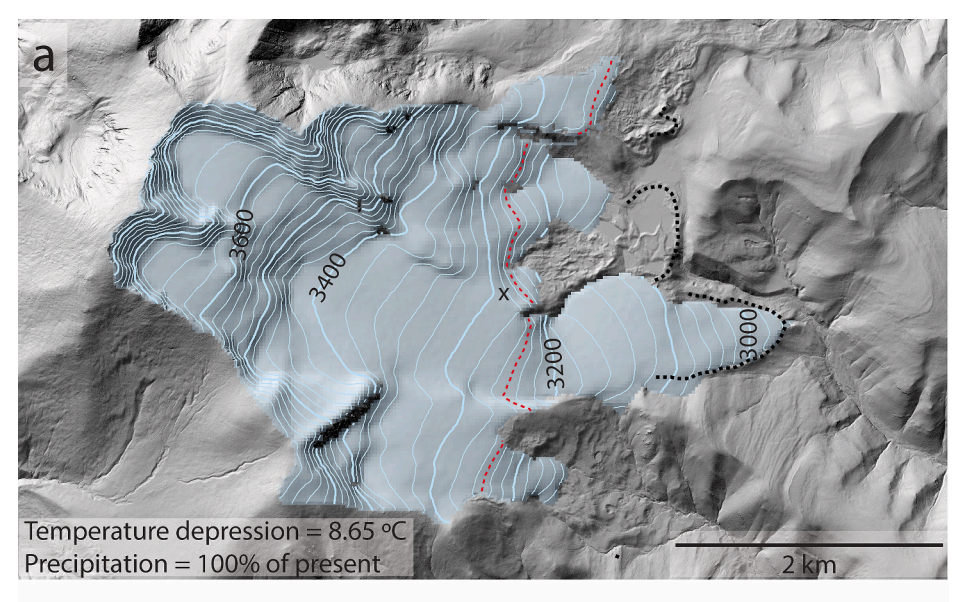
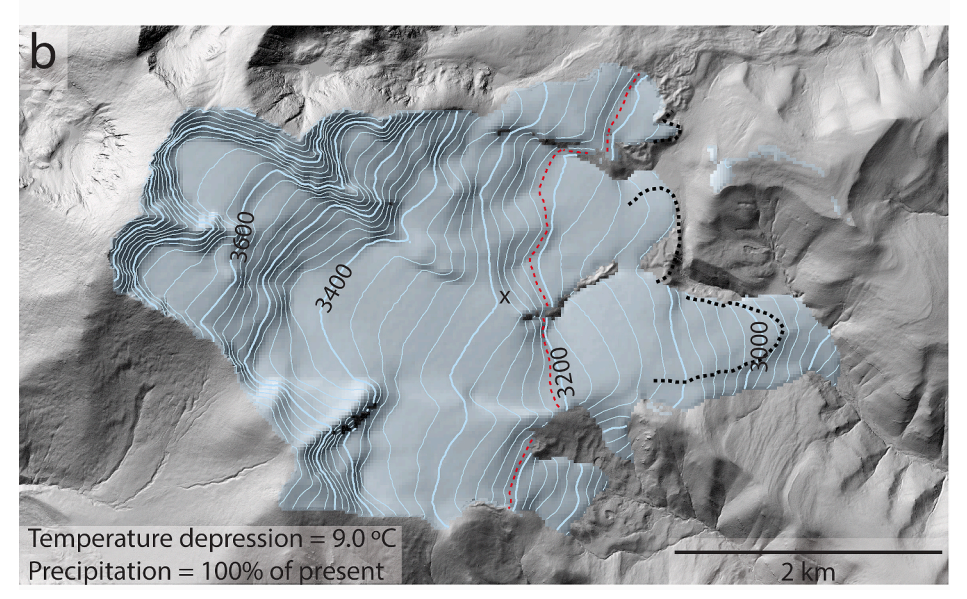


Fig. 8. Simulated glaciers representing the best fit to local Last Glacial Maximum latero-terminal moraines (indicated by black dashed lines) in the Winsor drainage. Both models assume no change in precipitation from modern conditions. Frame A shows simulation at 8.65 °C temperature depression from modern (1971-2000 CE) that results in the best fit to the main-valley moraines, but underpredicts the extent of ice in the northerntributary valley. Frame B shows simulation at 9.0 °C temperature depression that results in the best fit to the northern valley moraines but over predicts glacier extent in the main valley. Contour interval on simulated glacier surfaces is 20 m. Dashed red line is approximate position of the equilibrium line is each simulation. In both frames "x" indicates the area of probable cross-divide flow from the main Winsor valley into the northern tributary valley. (For interpretation of the references to colour in this figure legend, the reader is referred to the Web version of this article.)



mid-valley bench (Fig. 8a). In the main drainage itself, this simulation slightly underestimated the apparent ice thickness on the north side of the valley and overestimated it on the south side, resulting in a simulated limited overtopping of the south-side moraine. To fit the moraine complex on the northern mid-valley bench it was necessary to increase temperature depression to ~9.0 °C, as shown in Fig. 8b, which represents our best-fit simulation for the northern bench but significantly overestimates ice extent in the main valley. This difference in temperature depression necessary to simulate ice extent in the two areas is not surprising, as the modeling assumes a uniform elevation-dependence of climate and uniform glacier flow behavior across the model domain, which is certainly an oversimplification in even the small domain simulated here. The 0.3-0.4 $^{\circ}\text{C}$ difference between the two best-fit models is well within the overall uncertainty in the model (± 1.5 °C) discussed above. Based on the energy/mass balance simulations the glacier which best fits the main-valley moraines (Fig. 8a) would have had an LGM equilibrium line altitude (ELA) of ~3250 m, that providing the best fit to the northern-bench moraines (Fig. 8b) would have had an ELA of ~3210 m. Both of these values are somewhat lower than the 3310 m LGM ELA calculated by Meyer et al. (2014; Grant Meyer, personal communication, 2022) for the main-valley glacier based on accumulation-area ratio (AAR) methods with an assumed AAR of 0.65 (Porter, 1975; Meierding, 1982).

The climates that generated the simulated glaciers in Fig. 8 are not the only climates that could have could have sustained the mapped and dated LGM glaciers in the Winsor drainage. In these simulations only year-round temperatures were allowed to differ from modern conditions. Of course, any of the climate variable inputs in the energy/mass balance model could have differed from its present values at the LGM. Because temperature and precipitation are the first order controls on glacier mass balance (Ohmura et al., 1992; Oerlemans, 2001), we solved for the temperature depression that would have been necessary to sustain the LGM glaciers in mass-balance equilibrium over a range of input precipitation - expressed as multiples of modern precipitation - from half modern to twice modern. Results of these simulations for the main Winsor glacier and northern tributary glacier are shown in Fig. 9 and Table S-5. At half modern precipitation a temperature depression of 10.3-10.4 °C would have been necessary to sustain the main valley glacier, at twice modern precipitation a depression of ~6.3 °C could have sustained the glacier. Slightly greater temperature depression would have been necessary to sustain the north-tributary glacier in both cases (Fig. 9, Table S-5).

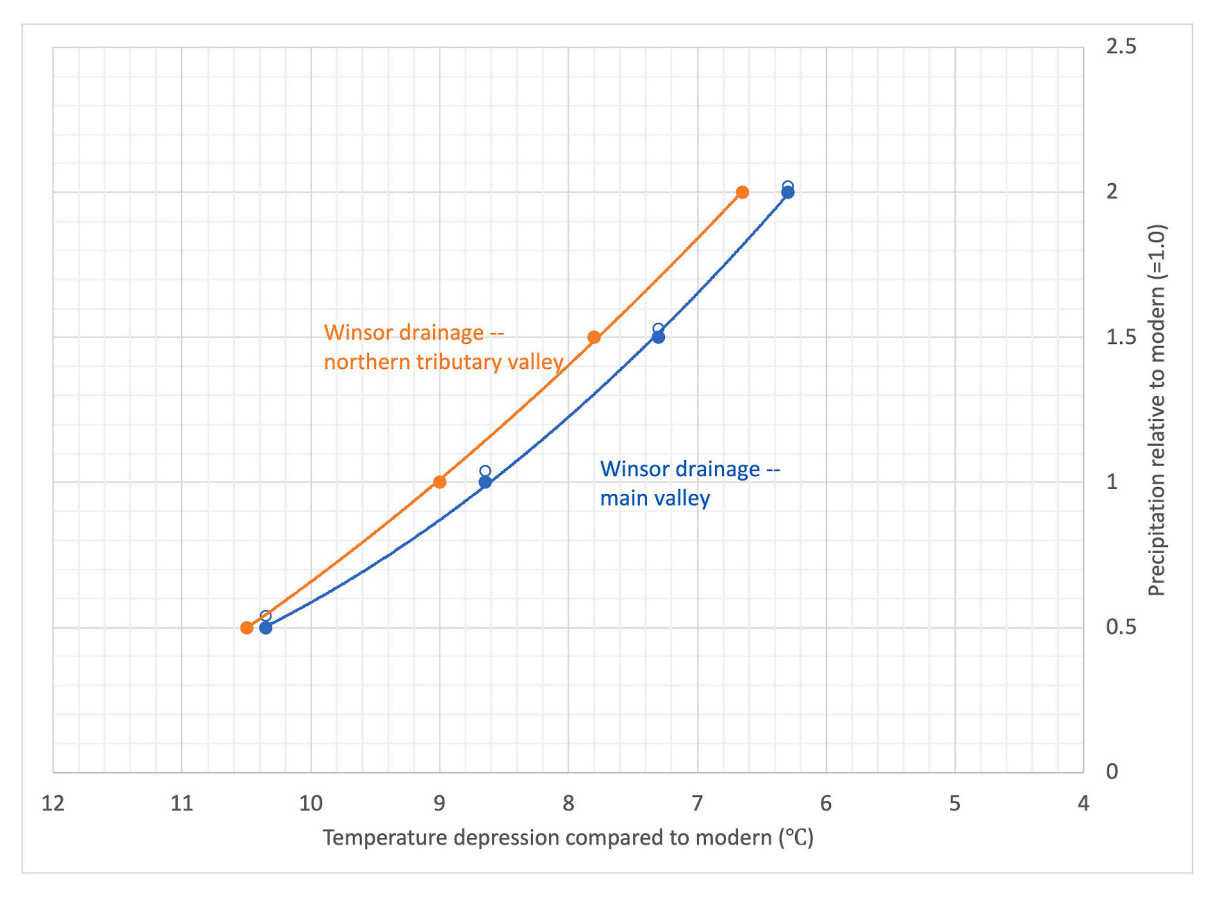


Fig. 9. Combinations of annual temperature and precipitation changes from modern (1971–2000 CE) that could have sustained glaciers in the main Winsor valley (blue) and the northern tributary valley (brown) at their mapped last glacial maximum extents. Circles indicate individual model simulations, lines are second-order polynomial best-fits to the simulations. Closed circles and best-fit lines indicate simulations with no change from modern precipitation seasonality. Open blue circles indicate fall-through-spring precipitation relative to modern in main valley simulations eliminating summer monsoon precipitation. (For interpretation of the references to colour in this figure legend, the reader is referred to the Web version of this article.)

The simulation results shown with closed circles and best-fit lines in Fig. 9 and in Table S-5 are based on an assumption that LGM precipitation seasonality did not differ from the modern. Sensitivity testing indicates that elimination of summer monsoon precipitation, by reducing July-through-September precipitation to the same levels as May–June precipitation, would have little effect on overall glacier mass balance (open circles in Fig. 9). To maintain the glaciers in mass-balance equilibrium at their LGM extents without monsoon precipitation would necessitate only very small amounts of additional fall-through-spring precipitation.

We did not undertake a systematic examination of the full range of conditions that could have sustained the glaciers at the extents indicated by the recessional moraines further upvalley. However, we found that in simulations run with 18 ka solar-insolation values but with no change in precipitation from modern conditions, temperature depressions required to produce glaciers in mass-balance equilibrium at the dated moraines upvalley from the LGM moraines (areas B and D in Fig. 6) would have been only $\sim\!0.3~^\circ\text{C}$ less than that required to sustain the downvalley LGM moraines. Alternatively, ice-marginal retreat from the LGM position to the recessional moraines could have been accomplished with a decrease in precipitation of $\sim\!10\%$ absent any temperature change.

6. Discussion

6.1. Ice flow in the Winsor drainage

Our field- and LiDAR-based mapping (Fig. 6) leaves open several

questions related to the dynamics of glaciers in the Winsor drainage – particularly to the interactions between main-valley ice and northern-tributary ice. How significant was the contribution of glaciers from the lower-altitude and smaller northern tributary valley to development of the glaciated landscape in the lower portions of the drainage? Are the outermost moraines on the northern portion of the mid-valley bench ("C" in Fig. 6) deposits of the northern-tributary glacier, or were they deposited by ice from the main valley? Consequently, are the moraines around Stewart Lake ("D" in Fig. 6) recessional, or do they represent the maximum stand of north-valley ice during the last glaciation? To what extent was upvalley cross-divide flow of ice from the main valley into the northern-tributary valley, and perhaps also into the Holy Ghost Creek drainage to the south, a major contributor to the glaciers in those smaller valleys, and was a cutoff of such cross-divide flow responsible for hummocky topography in the area southwest of Stewart Lake?

Modeled glacier geometry in the Winsor valley provides some answers to these questions. The model output displayed in Fig. 8b shows that ice on the northern portion of the mid-valley bench was sourced in the northern-tributary valley, rather than in the main valley, and the arcuate moraine complex in that area ("C" in Fig. 6), from which we have obtained multiple ¹⁰Be surface-exposure ages, was deposited by the northern-tributary glacier. Consequently the moraines impounding Stewart Lake ("D" in Fig. 6) must be recessional moraines. The reconstructions indicate that there was little, if any, confluence of ice from the two valleys on the midvalley bench. Both reconstructions indicate that the divides between the main valley and the northern tributary valley on one side and the Holy Ghost drainage on the other were covered with thin ice carapaces at the last glacial maximum. However,

as indicated by ice-surface contours, there appears to have been only limited flow across the divides. The one area where the contours suggest possibly significant cross-divide ice flow (x in Fig. 8a and b) is immediately up-ice from the area of apparent ice-stagnation topography southwest of Stewart Lake, suggesting that a cutoff of cross-divide ice flow during deglaciation may indeed have led to ice stagnation there.

6.2. Glacial chronology

Moraine-boulder exposure ages are generally interpreted to indicate the timing of initial recession of the active ice margin from the position of the moraine (Briner et al., 2005; Balco, 2011; Laabs et al., 2020). Following the practice used in the nearby Colorado Rocky Mountains (Briner, 2009; Leonard et al., 2017a, 2017b; Laabs et al., 2020; Schweinsberg et al., 2020), as well as by Marcott et al. (2019) in the upper portion of the Winsor drainage, we consider the mean age of all samples on a moraine, excluding obvious outliers, to represent the time of initial recession of ice from the moraine.

Results of ¹⁰Be surface-exposure analyses indicate that boulders on the outermost mapped moraines were deposited during the last ("Pinedale") glaciation. None of the samples yielded ages from the penultimate ("Bull Lake") glaciation, although previous work in the drainage (Wesling, 1987, 1988) suggested that some of the sampled moraines dated from that glaciation. Four of the five boulders sampled from the outermost moraine complexes yielded ¹⁰Be exposure ages ranging from 19.1 \pm 0.5 ka to 24.0 \pm 0.9 ka, with a mean of 21.2 \pm 2.0 ka (1σ standard deviation), the fifth (sample WIN12-03) yielding an age of 39.5 \pm 0.8 ka. This last age, which is more than nine standard deviations beyond the mean of the other four ages, likely reflects an inherited inventory of ¹⁰Be in the boulder at the time of its deposition on the moraine and thus does not reflect the age of the moraine. The presence of such outliers is not uncommon. A compilation of exposure ages from boulders on alpine moraines throughout the western United States indicates that approximately 12% of those moraines contain one or more boulders that yielded old outlier ages (Table S-1 in Laabs et al., 2020). Considered together the four remaining samples suggest strongly that these boulders were deposited, and that initial ice recession from the moraines began, during the global LGM interval (26-19ka; Clark et al., 2009). The relatively wide scatter of ages among the four boulders, along with the fact that the fifth boulder yielded an age of nearly 40 ka, much older than the global LGM, but still significantly younger than the penultimate glaciation (~130–140 ka – Laabs et al., 2020), indicates that inheritance of a pre-deposition 10Be inventory and/or post-depositional shielding may have influenced the 10Be concentrations, and thus the assigned ages, of some or all of the samples. Nonetheless, the ages almost certainly indicate that initial recession from the outermost moraines occurred during the interval of the global Last Glacial Maximum.

Exposure ages on recessional-moraine boulders present a more complex picture. In the main valley the three boulders dated all postdate 20 ka, consistent with their position upvalley from or inside the outer moraine. However, there is not a consistent pattern of upvalley younging, and the youngest age (15.3 \pm 0.6 – sample WIN12-11), on the moraine crest closest to the outer moraine, is indistinguishable from the age of 15.1 \pm 0.4 assigned by Marcott et al. (2019) to moraines far upvalley based on multiple ¹⁰Be exposure ages (Fig. 7). We suggest that the surprisingly young age for sample WIN12-11 is a result of either post-depositional shielding or weathering of the sample. In the northern tributary drainage the recessional moraine ages are similarly puzzling. One of two boulders there yielded an age of 17.5 \pm 0.5 (sample WIN12-06), consistent with its position not far inside the outer moraine complex, but a second recessional-moraine boulder yielded an age of 22.7 ± 0.7 (sample WIN12-07), older than two of the four boulders analyzed in the outer moraine complex downvalley, suggesting that it too may contain an inherited inventory of ¹⁰Be. Pooling the ages of all five boulders on the recessional moraines yields a mean age of 18.6 \pm

2.8 ka (1 σ). Eliminating the two suspect ages yields a mean for the remaining three samples of 18.3 \pm 1.3 ka (1 σ).

Although there is considerable variability in the ^{10}Be exposure ages, our preferred interpretation is that the initial recession from the local last glacial maximum occurred at 21.2 ± 2.0 ka, during the global LGM, and that at 18.3 ± 1.3 ka ice began to recede from the recessional-moraine positions a short distance upvalley. The initial recession, before about 18 ka, involved a less than 20% reduction of glacier length compared to the LGM extent in both valleys. By about 15 ka, the ice margin had retreated to the Lake Katherine cirque, nearly deglaciating the entire main valley, with remaining glacier length less than 15% of its LGM extent. Recession from the moraines impounding Lake Katherine began at 15.1 ± 0.4 ka (Marcott et al., 2019).

Our new exposure ages suggest that the initiation of sedimentation at "Bog B-1" (Fig. 3) on the midvalley bench (Armour et al., 2002; Jiménez-Moreno et al., 2008) postdated deglaciation of the area by several thousand years, consistent with past observations that basal ages lakes and bogs may be significantly postdate deglaciation (Davis and Davis, 1980). The Marcott et al. (2019) ages from the Lake Katherine moraines indicate that any glacial response to the climate fluctuations documented in the "Bog B-1" cores by Armour et al. (2002) and Jiménez-Moreno et al. (2008) must have been limited to the upper portions of the Lake Katherine cirque.

The pattern of a maximum local ice extent during the global LGM interval, with ice then either remaining nearly as extensive, or readvancing to nearly the same extent, several thousand years later, has also been recognized further north in the U.S. Rocky Mountains (Ward et al., 2009; Leonard et al., 2017b; Laabs et al., 2020). In a few areas, particularly in the northernmost sections of the range, this later, post-global LGM stand was actually the local maximum (Quirk et al., 2022), but in other areas, moraines from both periods are preserved (e.g. Tulenko et al., 2020).

The chronology of deglaciation from the Winsor drainage is also consistent, given current chronological uncertainties, with evidence of changing late Pleistocene lake levels in the nearby Estancia Basin (Fig. 1), recently detailed by Menking et al. (2018). High lake levels prevailed during the LGM, between about 22 and 20 ka (Fig. 10), based on a combined radiocarbon and U-Th age model. These were followed at about 20 ka by a drop to intermediate lake levels, which persisted until about 18 ka. We note that during this interval age control in the Estancia Basin record is dominantly based on radiocarbon ages on ostracodes (Menking et al., 2018). This initial drop in lake levels appears to have occurred slightly later than the initiation of deglaciation in the Winsor drainage indicated by the 21.2 \pm 2.0 ka mean exposure age on the outermost moraines in the Winsor drainage, although the timing is not inconsistent given current chronological uncertainties in both datasets. A subsequent drop to low levels of Lake Estancia at around 18 ka corresponds closely in time with the apparent beginning of ice recession from the Winsor basin recessional moraines (18.3 \pm 1.3 ka), which initiated the main phase of deglaciation of the basin (Fig. 10). The final Late Pleistocene recession of ice from the moraines impounding Lake Katherine at 15.1 \pm 0.4 ka (Marcott et al., 2019) is coincident with a subsequent major drying event at Estancia beginning about 15 ka.

6.3. Climate of the last glacial maximum

Our model simulations indicate that, if total precipitation and precipitation seasonality were the same as modern, a temperature depression of 8.6–9.0 °C would have been necessary to sustain glaciers in the Winsor Creek drainage at their LGM extents. Lesser or greater temperature depressions would have been necessary if precipitation at the LGM were more or less. In the Nambe Creek drainage immediately to the southwest of the Winsor Creek drainage (Fig. 2), work using an earlier version of the model used in this study (Jacobsen et al., 2010) suggested a similar LGM temperature depression, of 8.4 °C, again assuming no change from modern precipitation.

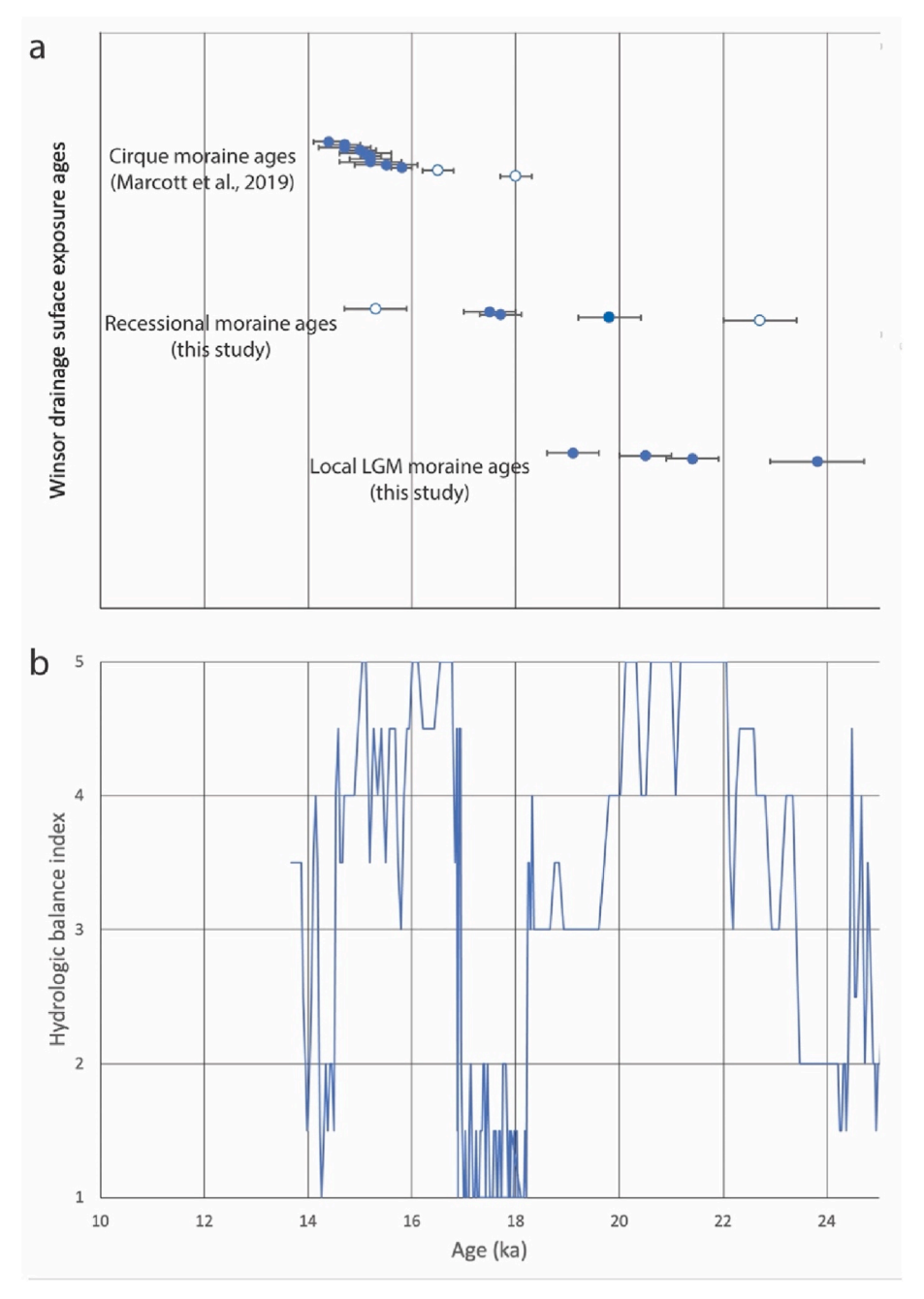


Fig. 10. Comparison of Winsor drainage glacial sequence with Lake Estancia hydrologic balance (Menking et al., 2018) 25–14 ka. (a) $^{10} \mbox{Be}$ ages from moraine boulders in the Winsor drainage. Individual boulder ages are plotted with 1σ internal (analytical) uncertainty indicated by error bars. Probable outliers are indicated by open circles. One additional outlier in the local LGM moraine complex yielded an age of 39.5 ± 0.8 ka. (b) Hydrologic balance index for Lake Estancia. The index is a semi-quantitative indication of lake water levels based on a combination of core and outcrop sedimentological characteristics, with higher numbers corresponding to higher lake stands.

Both low-altitude proxy climate reconstructions and climate-model output suggest, however, that during the LGM climate in New Mexico was somewhat wetter than at present, and that precipitation seasonality may have also changed. Early work by Leopold (1951) and Antevs (1954), combining lake water-balance calculations with temperature estimates based on assumed late Pleistocene snowline depression, suggested that both temperature depression and precipitation increase were necessary to explain high late Pleistocene levels of Lake Estancia (Fig. 1), a conclusion also reached by Menking et al. (2004) based on hydrological modeling. Oxygen-isotope timeseries from the Fort Stanton Cave (Fig. 1) speleothem (Asmerom et al., 2010) indicate that during the interval of the LGM Pacific-sourced winter precipitation increased significantly relative to monsoonal summer precipitation. Most other proxies and climate models also suggest an increase in winter precipitation in the southwestern United States at the LGM (Oster et al., 2015; Oster and Ibarra, 2019; Lora and Ibarra, 2019). The amount of LGM

summer precipitation, and especially the persistence of the monsoon, is less clear in climate-model simulations and proxy data. Some recent models indicate that a strong monsoon persisted through the LGM (Lora, 2018), while others indicate a reduction of monsoonal precipitation, particularly north of about 35°N latitude – including the present study area (Bhattacharya et al., 2017). Similarly while proxy data suggest the persistence of monsoon precipitation in some parts of the southwestern United States, spatial comparisons suggest that north of about 35°N LGM summer moisture transport appears to have been reduced (Holmgren et al., 2007).

Model sensitivity tests involving suppressed monsoon precipitation suggest that the Winsor glaciers were quite insensitive to summer precipitation. A complete suppression of monsoon precipitation would necessitate only a very small counterbalancing increase in fall-through-spring precipitation to maintain the glaciers in mass balance equilibrium. Consequently, the values for precipitation necessary to sustain the

glaciers at particular LGM temperature depressions presented in Fig. 9 (closed circles) and Table S-5, although they were calculated assuming no change in precipitation seasonality, are very close to, if a few percent less than, the fall-through-spring precipitation amounts that would have been necessary even with a complete suppression of the monsoon at the LGM.

Oster et al. (2015) compared output from the eight 21 ka climate models incorporated in PMIP 3 (Paleoclimate Model Intercomparison Project Phase III) with LGM precipitation proxies across western North America, identifying five of the eight models that provided best fits to the proxies. Output from those five models was interpolated to the Winsor drainage study area, using bilinear interpolation methods (Oster and Ibarra, 2019), and indicate an ensemble mean 21 ka annual temperature depression of 7.9 \pm 2.2 $^{\circ}\text{C}$ (range 4.9–10.9 $^{\circ}\text{C})$ compared with pre-industrial (PI) temperature, coupled with 21 ka annual precipitation equal to 120 \pm 24% (range 98–152%) of PI precipitation. Focusing on the seasonal intervals that likely most strongly influence paleoglacier mass balance, the ensemble mean indicates a 21-ka summer (June through August) temperature depression of 7.3 \pm 2.6 °C (range 3.8–9.7 °C) at 21 ka coupled with fall-through-spring (September through May) precipitation of 111 \pm 24% (range 92–139%) of PI. The TraCE 21 ka time-dependent (CCSM3) indicates model also wetter-than-preindustrial LGM. Model output interpolated to the Winsor drainage indicate a mean annual LGM temperature (calculated as mean temperature during the 22-20 ka interval) 7.0 °C colder than the PI temperature (defined as the mean temperature during the 1745-1855 CE interval) and that LGM annual precipitation was 113% of PI annual precipitation over the same comparison time periods. Seasonal output from the TraCE 21 ka model indicates an LGM summer temperature depression of 6.0 °C, coupled with 126% of PI fall-through-spring precipitation.

Although the climate models suggest a wide range of possible LGM conditions, and although we estimate that there is about a $\pm 1.5\,^{\circ}$ C uncertainty in our glacier-model paleotemperature estimates for any particular paleoprecipitation value, the climate model ensemble means, either annual or seasonal, are comparable to glacier model output

(Fig. 11). The fact that climate-model simulations generally appear to indicate slightly less LGM temperature depression than do our glacier models may be explained at least in part by the fact that for the glacier models, LGM temperature depressions are calculated with respect to "modern" (1971-2000 CE) conditions, whereas for the climate models, LGM temperature depression is calculated with respect to slightly cooler pre-industrial (i.e. ~1850 CE) conditions. It is also possible that LGM regional temperature depression was greater at high altitude than at low altitude as has been noted in the tropics (Tripati et al., 2014). Taken together the glacier-model and climate-model outputs suggest a most likely LGM temperature depression of about 8 °C, coupled with somewhat higher (\sim 110–125%) than modern precipitation. Because the persistence or reduction of the summer monsoon appears to have little effect on the simulated glacier mass balance, and because the strength of the monsoon in northern New Mexico at the LGM remains a topic of uncertainty, it is probably best to interpret this inferred LGM increase in precipitation as an indication of increases in fall-through-spring precipitation.

While our LGM glacier model results from the southernmost Sangre de Cristo Mountains in New Mexico appear broadly consistent with both climate models and other nearby climate proxies, they suggest a more profound change there between LGM and modern conditions than does our glacier modeling further north, in the Colorado Sangre de Cristo Mountains. Employing the same Plummer and Phillips (2003) glacier model in the Cuelebra Peak area (~37.1°N, Fig. 1) about 150 km north along range from the current study area, a temperature depression of only 6.3 °C would have been necessary to sustain the mapped LGM glacier assuming no change from modern precipitation (Erica Evans, personal communication 2015), and in the Crestone Peaks area (~38.0°N, Fig. 1), about 230 km north of the current study area, only 5.0-5.1 °C depression would have been necessary, again assuming modern precipitation (Leonard et al., 2017a). Climate models, virtually without exception, indicate that the magnitude of LGM temperature depression compared to modern conditions, decreased southward in the Rocky Mountain region with increasing distance from the margin of the Laurentide Ice Sheet, in apparent conflict with our glacier model results.

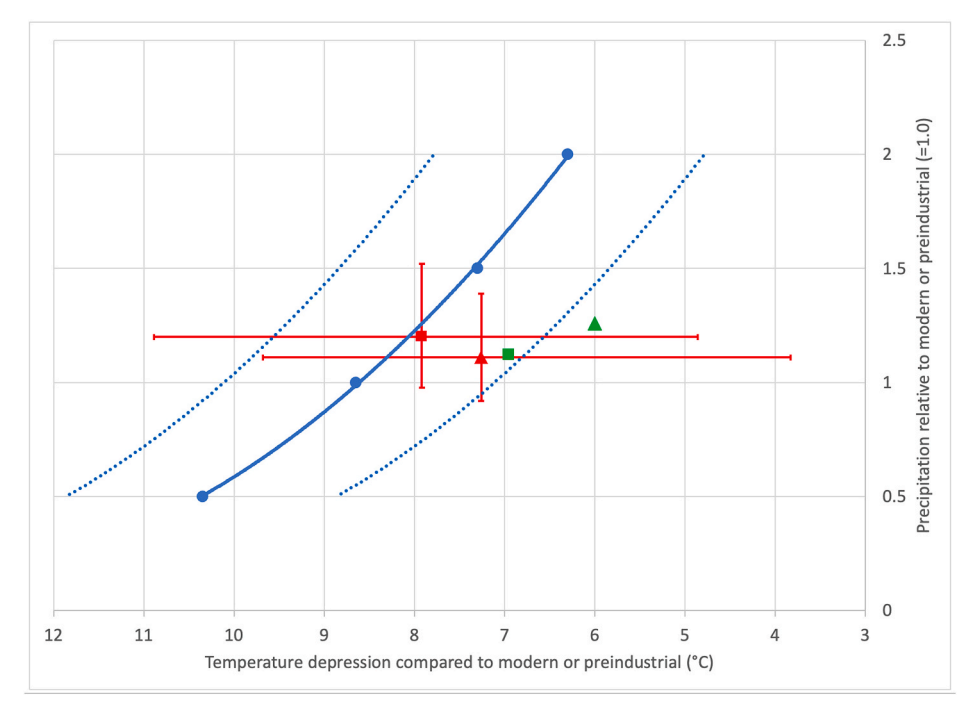


Fig. 11. Comparison of LGM temperature and precipitation conditions indicated by glacier-model and global climate-model simulations. Solid blue curve represents the combinations of temperature depression and precipitation relative to modern (1971-2000 CE) that could have sustained the LGM main Winsor Valley glacier in mass-balance equilibrium based on glacier-model simulations. Dashed blue curves bound a ± 1.5 °C envelope of uncertainty in model temperature estimates for a specified precipitation relative to modern. Red symbols indicate 21ka temperature and precipitation values from the five PMIP3 climate models identified by Oster et al. (2015) as providing the best fits to proxy precipitation data, interpolated to the Winsor drainage. Square symbol indicates five-model means of annual temperature depression and precipitation relative to pre-industrial conditions. Triangle symbols indicate five-model means of summer temperature depression and fall-through-spring precipitation. Error bars indicate the range of values produced by the five PMIP3 models. Green symbols indicate the LGM annual (square) and seasonal (triangle) temperature depression compared to pre-industrial conditions based on TraCE 21ka model output, interpolated to the Winsor drainage. See text for details of how these values were computed. (For interpretation of the references to colour in this figure legend, the reader is referred to the Web version of this article.)

However, both proxy data and climate models generally indicate drier-than-modern LGM conditions in the northern US Rocky Mountains and wetter-than-modern LGM conditions in the southern Rocky Mountains, with the boundary between drier conditions to the north and wetter conditions to the south generally located somewhere in Colorado (Oster et al., 2015). Thus, it seems likely that at least part of the apparent discrepancy between the temperature-depression patterns suggested by our glacier modeling and that suggested by climate-model output may be explained by reduced LGM precipitation in the Colorado Sangre de Cristo coupled with increased LGM precipitation in the New Mexico Sangre de Cristo.

This more profound change from modern conditions necessary to explain the extent of LGM glaciation in the southernmost Rocky Mountains than that necessary further north which is indicated by our paleoglacier simulations is consistent with patterns in LGM glacier equilibrium-line altitudes (ELAs). As noted above (section 5.3) energy/ mass balance simulations indicate an LGM ELA of 3210-3250 m in the Winsor drainage, whereas in the Crestone Peaks area of the northern Sangre de Cristo in Colorado the same methods yield an LGM ELA of \sim 3425 m (Leonard et al., 2017a), which is 175–215 m higher. Similarly, the 3310 m LGM ELA calculated for the Winsor drainage using accumulation-area-ratio methods (Meyer et al., 2014; Grant Meyer, personal communication, 2022) is 250-400 m lower than those calculated by Refsnider et al. (2009) for the Crestone Peaks glaciers using the same methods. Absent modern glaciers it is not possible to assess modern ELAs and LGM ELA depression compared to the modern. However, the pattern of lower LGM ELAs to the south, higher to the north contrasts with the expected general increase in ELAs with decreasing latitude, and is consistent with increased LGM precipitation in the south and possibly decreased precipitation in the north being key factors in LGM glacier mass balances.

Our model results strongly suggest an LGM increase in precipitation in the southernmost Rocky Mountains, at least during the fall-throughspring seasons, consistent with most climate model and proxy studies. Such an increase, coupled with speleothem oxygen-isotope data indicating a dominance of Pacific-sourced moisture during the LGM (Asmerom et al., 2010), would be consistent with climate models that indicate a southward displacement of the mean position of the winter storm track across the western United States during the LGM, bringing increased cyclonic precipitation to the U.S. Southwest and southern Rocky Mountains (e.g. Kutzbach and Wright, 1985; Thompson et al., 1993; Bartlein et al., 1998; Laîné et al., 2009), and/or an increased intensity and penetration of winter-season Pacific atmospheric rivers into the southwest (Lora et al., 2017). Due to the apparent insensitivity of the modeled glaciers to summer precipitation, however, our results do not provide insight into the currently unresolved question of the persistence or suppression of the summer monsoon during the LGM

7. Conclusions

CRN surface-exposure dating of late Pleistocene deposits in the Winsor Creek drainage of the southernmost Sangre de Cristo Mountains indicates that the glaciers were at their maximum stand of the last glaciation until about 21.2 \pm 2.0 ka, providing the first numerical ages for the local last glacial maximum in the southernmost Rocky Mountains. If precipitation amount and seasonality at that time were the same as modern, a temperature depression of 8.6-9.0 °C would have been necessary to sustain the LGM glaciers. However, based on evidence from other proxy records, particularly speleothem and lake-level records, that precipitation at that time appears to have been somewhat higher than present, a somewhat smaller temperature depression would have sustained the glaciers. Combining our glacier-model results with climatemodel output suggests that an LGM temperature depression of ~8 °C, combined with a 10-25% increase in precipitation, at least during the fall-through-spring seasons, is likely a better estimate of the conditions leading to the LGM glaciation. This enhanced fall-through-spring precipitation was likely a result of the southward displacement of mean winter storm track during the LGM and/or increased intensity of Pacific atmospheric rivers penetrating into the southwest US. Until about 18.3 \pm 1.3 ka, the glaciers in the drainage remained close to their maximum extent, suggesting that only a few tenths of a degree temperature rise and/or a small amount of drying ($\sim\!10\%$ precipitation decrease) had occurred by that time. The main deglaciation of the valley occurred subsequently and the drainage was nearly completely deglaciated by about 15ka.

Declaration of competing interest

The authors declare that they have no known competing financial interests or personal relationships that could have appeared to influence the work reported in this paper.

Data availability

Data will be made available on request.

Acknowledgements

EL thanks John Wesling for introducing him to the study area on a 1987 Friends of the Pleistocene field trip, and Peter Fawcett for joining us in the field in summer 2009 and providing an update on work done with students there over the previous decade. Colorado College students Robert Jacobsen, Ben Mackall, Jessica Treanton and Ryan Gall assisted with field work. Ryan also worked with on processing ¹⁰Be samples along with SUNY-Geneseo students Elizabeth (Huss) Sanguinito, Brendon Quirk, Alec Spears, Douglas Steen, and Katherine Truong. We thank Erica Evans and Grant Meyer for allowing us to make reference to their unpublished results in this paper. We also thank two anonymous reviewers for their very perceptive comments which resulted in considerable improvements to the manuscript. Financial support was provided by the United States National Science Foundation [NSF/GLD 1024838 and NSF/GLD 1024852] to EL and BL.

Appendix A. Supplementary data

Supplementary data to this article can be found online at https://doi.org/10.1016/j.qsa.2023.100070.

References

Allen, B.D., 2005. Ice age lakes in New Mexico. Ice Age vegetation and flora of New Mexico. In: Lucas, S.G., Morgan, G.S., Zeigler, K.E. (Eds.), New Mexico's Ice Ages: New Mexico Museum of Natural History and Sciences Bulletin, vol. 28, pp. 107–113.

Allen, B.D., Anderson, R.Y., 2000. A continuous, high-resolution record of late Pleistocene climate variability from the Estancia Basin, New Mexico. Geol. Soc. Am. Bull. 112, 1444–1458. https://doi.org/10.1130/0016-7606(2000)112<1444: ACHRRO>2.0.CO:2.

Anderson, L.S., Roe, G.H., Anderson, R.S., 2014. The effects of interannual climate variability on the moraine record. Geology 42, 55–58. https://doi.org/10.1130/ G34791.1.

Antevs, E., 1935. The occurrence of flints and extinct animals in pluvial deposits near Clovis, New Mexico, Part II: age of the Clovis lake clays. Proc. Acad. Nat. Sci. Phila. 87, 304–312.

Antevs, E., 1954. Climate of New Mexico during the last glacio-pluvial. J. Geol. 62, 182–191.

Armour, J., Fawcett, P.J., Geissman, J.W., 2002. 15 ky paleoclimatic and glacial record from northern New Mexico. Geology 30, 723–726. https://doi.org/10.1130/0091-7613(2002)030<0723:KYPAGR>2.0.CO;2.

Asmerom, Y., Polyak, V.J., Burns, S.J., 2010. Variable winter moisture in the southwestern United States linked to rapid glacial climate shifts. Nat. Geosci. 3, 114–117. https://doi.org/10.1038/NGEO754.

Asmerom, Y., Polyak, V.J., Lachniet, M.S., 2017. Extrapolar climate reversal during the last deglaciation. Sci. Rep. 7, 1–7. https://doi.org/10.1038/s41598-017-07721-8.

Balco, G., 2011. Contributions and unrealized potential contributions of cosmogenicnuclide exposure dating to glacier chronology, 1990–2010. Quat. Sci. Rev. 30, 3–27. https://doi.org/10.1016/j.quascirev.2010.11.003.

Balco, G., Stone, J.O., Lifton, N.A., Dunai, T.J., 2008. A complete and easily accessible means of calculating surface exposure ages or erosion rates from 10Be and 26Al

- measurements. Quat. Geochronol. 3, 174–195. https://doi.org/10.1016/j.
- Bartlein, P.J., Anderson, K.H., Anderson, P.M., Edwards, M.E., Mock, C.J., Thompson, R. S., Webb, R.S., Webb III, T., Whitlock, C., 1998. Paleoclimate simulations for North America over the past 21,000 years: features of the simulated climate and comparisons with paleoenvironmental data. Quat. Sci. Rev. 17, 549–585.
- Bhattacharya, T., Tierney, J.E., DiNezio, P., 2017. Glacial reduction of the North American Monsoon via surface cooling and atmospheric ventilation. Geophys. Res. Lett. 44, 5113–5122. https://doi.org/10.1002/2017GL073632.
- Birkel, S.D., Putnam, A.E., Denton, G.H., Koons, P.O., Fastook, J.L., Putnam, D.E., Maasch, K.A., 2012. Climate inferences from a glaciological reconstruction of the late Pleistocene Wind River Ice Cap, Wind River Range, Wyoming. Arctic Antarct. Alpine Res. 44, 265–276. https://doi.org/10.1657/1938-4246-44.3.265.
- Brakenridge, G.R., 1978. Evidence for a cold, dry full-glacial climate in the American Southwest. Quat. Res. 9, 22–40.
- Briner, J.P., 2009. Moraine pebbles and boulders yield indistinguishable ¹⁰Be ages: a case study from Colorado, USA. Quat. Geochronol. 4, 299–305. https://doi.org/10.1016/j.quageo.2009.02.010.
- Briner, J.P., Kaufman, D.S., Manley, W.F., Finkel, R.C., Caffee, M.W., 2005. Cosmogenic exposure dating of late Pleistocene moraine stabilization in Alaska. Geol. Soc. Am. Bull. 117, 1108–1120. https://doi.org/10.1130/B25649.1.
- Brugger, K.A., 2010. Climate in the southern Sawatch Range and Elk Mountains, Colorado, USA, during the Last Glacial Maximum: inferences using a simple degreeday model. Arctic Antarct. Alpine Res. 42, 164–178. https://doi.org/10.1657/1938-4246-42.2.164.
- Brugger, K.A., Laabs, B., Reimers, A., Bensen, N., 2018. Late Pleistocene glaciation in the Mosquito Range, Colorado, USA: chronology and climate. J. Quat. Sci. 34, 187–202. https://doi.org/10.1002/jqs.3090.
- Brugger, K.A., Ruleman, C.A., Caffee, M.W., Mason, C.C., 2019. Climate during the Last Glacial Maximum in the northern Sawatch Range, Colorado. Quaternary 2, 36. https://doi.org/10.3390/quat2040036.
- Brugger, K.A., Leonard, E.M., Refsnider, K.A., Dolan, P., 2021. Climate on the Blanca Massif, Sangre de Cristo Mountains, Colorado, USA, during the Last Glacial Maximum. Quaternary 4. https://doi.org/10.3390/quat4030027.
- Clark, P.U., Dyke, A.S., Shakun, J.D., Carlson, A.E., Clark, J., Wohlfarth, B., Mitrovica, J. X., Hostetler, S.W., McCabe, A.M., 2009. The Last Glacial Maximum. Science 325, 710–714. https://doi.org/10.1126/science.1172873.
- Clisby, K.H., Sears, P.B., 1956. San Augustin plains—Pleistocene climatic changes. Science 124, 537–539.
- COHMAP Members, 1988. Climatic changes of the last 18,000 years: observations and model simulations. Science 241, 1043–1052.
- Daly, C., Halbleib, M., Smith, J.I., Gibson, W.P., Doggett, M.K., Taylor, G.H., Curtis, J., Pasteris, P.P., 2008. Physiographically sensitive mapping of climatological temperature and precipitation across the conterminous United States. Int. J. Climatol. 28, 2031–2064. https://doi.org/10.1002/joc.1688.
- Davis, P.T., Davis, R.B., 1980. Interpretation of minimum-limiting radiocarbon dates for deglaciation of Mt.Katahdin area, Maine. Geology 8, 396–400.
- Dühnforth, M., Anderson, R.S., 2011. Reconstructing the glacial history of Green Lakes valley, North Boulder Creek, Colorado Front Range. Arctic Antarct. Alpine Res. 43, 527–542. https://doi.org/10.1657/1938-4246-43.4.527.
- Farinotti, D., 2017. On the effect of short-term climate variability on mountain glaciers: insights from a case study. J. Glaciol. 59, 992–1006. https://doi.org/10.3189/ 2013.16013.1080
- Hall, S.A., Lucas, S.G., Morgan, G.S., Zeigler, K.E., 2005. Ice Age vegetation and flora of New Mexico. In: Lucas, S.G., Morgan, G.S., Zeigler, K.E. (Eds.), New Mexico's Ice Ages, New Mexico Museum of Natural History and Sciences Bulletin, vol. 28, pp. 171–183.
- Holmgren, C.A., Norris, J., Betancourt, J.L., 2007. Inferences about winter temperature and summer rains from the late Quaternary record of C4 perennial grasses and C3 desert shrubs in the northern Chihuahuan Desert. J. Quat. Sci. 22, 141–161. https:// doi.org/10.1002/jqs.1023.
- Hudson, A.M., Hatchett, B.J., Quade, J., Boyle, D.P., Bassett, S.D., Ali, G., De los Santos, M.G., 2019. North-south dipole in winter hydroclimate in the western United States during the last deglaciation. Sci. Rep. 9 (1), 1–12. https://doi.org/10.1038/ s41598-019-41197-y.
- Hutter, K., 1983. Theoretical Glaciology: Material Science of Ice and the Mechanics of Glaciers and Ice Sheets. Reidel, Dordrecht, p. 510p.
- Ibarra, D.E., Oster, J.L., Winnick, M.J., Caves Rugenstein, J.K., Byrne, M.P., Chamberlain, C.P., 2018. Warm and cold wet states in the western United States during the Pliocene–Pleistocene. Geology 46, 355–358. https://doi.org/10.1130/ G39962.1.
- Jacobsen, R.E., Leonard, E.M., Plummer, M.A., 2010. Last Glacial Maximum climate in the southernmost Rocky Mountains, USA. Geological Society of America Annual Meeting Abstracts.
- Jarosch, A.H., Schoof, C.G., Anslow, F.S., F, S., 2013. Restoring mass conservation to shallow ice flow models over complex terrain. Cryosphere 7, 229–240. https://doi. org/10.5194/tc-7-229-2013.
- Jiménez-Moreno, G., Fawcett, P.J., Anderson, R.S., 2008. Millennial-and centennial-scale vegetation and climate changes during the late Pleistocene and Holocene from northern New Mexico (USA). Quat. Sci. Rev. 27, 1442–1452. https://doi.org/ 10.1016/j.quascirev.2008.04.004.
- Kinworthy, B., 2016. New Mexico Rock Glacier Inventory: Analysis of Geomorphology and Paleogeography. MS thesis University of New Mexico, Albuquerque, p. 136. https://digitalrepository.unm.edu/geog_etds/27. (Accessed 8 November 2022).
- Kohl, C.P., Nishiizumi, K., 1992. Chemical isolation of quartz for measurement of in-situproduced cosmogenic nuclides. Geochem. Cosmochim. Acta 56 (9), 3583–3587.

- Kutzbach, J.E., Wright Jr., H.E., 1985. Simulation of the climate of 18,000 years BP: results for the North American/North Atlantic/European sector and comparison with the geologic record of North America. Quat. Sci. Rev. 4, 147–187.
- Laabs, B.J.C., Plummer, M.A., Mickelson, D.M., 2006. Climate during the last glacial maximum in the Wasatch and southern Uinta Mountains inferred from glacier modeling. Geomorphology 75, 300–317. https://doi.org/10.1016/j. geomorph.2005.07.026.
- Laabs, B.J., Munroe, J.S., Best, L.C., Caffee, M.W., 2013. Timing of the last glaciation and subsequent deglaciation in the Ruby Mountains, Great Basin, USA. Earth Planet Sci. Lett. 361, 16–25. https://doi.org/10.1016/j.epsl.2012.11.018.
- Laabs, B.J.C., Licciardi, J.M., Leonard, E.M., J, M., Marchetti, D.W., Munroe, J.S., 2020. Updated cosmogenic chronologies of Pleistocene mountain glaciation in the western United States and associated paleoclimate inferences. Quat. Sci. Rev. 242 https://doi.org/10.1016/j.quascirev.2020.106427.
- Laîné, A., Kageyama, M., Salas-Mélia, D., Voldoire, A., Rivière, G., Ramstein, G., Planton, S., Tyteca, S., Peterschmitt, J.Y., 2009. Northern hemisphere storm tracks during the last glacial maximum in the PMIP2 ocean-atmosphere coupled models: energetic study, seasonal cycle, precipitation. Clim. Dynam. 32, 593–614.
- Le Meur, E., Vincent, C., 2003. A two-dimensional shallow ice-flow model of glacier de Saint-Sorlin, France. J. Glaciol. 49, 527–538. https://doi.org/10.3189/ 172756503781830421.
- Leonard, E.M., Laabs, B.J., Plummer, M.A., Kroner, R.K., Brugger, K.A., Spiess, V.M., Refsnider, K.A., Xia, Y., Caffee, M.W., 2017a. Late Pleistocene glaciation and deglaciation in the Crestone Peaks area, Colorado Sangre de Cristo Mountains chronology and paleoclimate. Quat. Sci. Rev. 158, 127–144. https://doi.org/10.1016/j.quascirev.2016.11.024.
- Leonard, E.M., Laabs, B.J.B., Schweinsberg, A.D., Russell, C.M., Briner, J.B., Young, N.E., 2017b. Deglaciation of the Colorado Rocky Mountains following the last glacial maximum. Cuadernos de Investigacion Geografica 43, 497–526. https://doi.org/ 10.18172/cig.3234.
- Leonard, E.M., Plummer, M.A., Laabs, B.J., 2019. The significance of interannual variability for paleoclimatic reconstructions from moraine sequences. In:

 International Union for Quaternary Research, XXth International Congress.
- Leopold, L.B., 1951. Pleistocene climate in New Mexico. Am. J. Sci. 249, 152–168.
- Leysinger Vieli, G.J.-M., Gudmundsson, G.H., 2004. On estimating length fluctuations of glaciers caused by changes in climatic forcing. J. Geophys. Res. 109, F01007 https:// doi.org/10.1029/2003JF000027.
- Licciardi, J.M., Pierce, K.L., 2018. History and dynamics of the Greater Yellowstone Glacial System during the last two glaciations. Quat. Sci. Rev. 200, 1–33. https://doi. org/10.1016/j.quascirev.2018.08.027.
- Lifton, N., Sato, T., Dunai, T.J., 2014. Scaling in situ cosmogenic nuclide production rates using analytical approximations to atmospheric cosmic-ray fluxes. Earth Planet Sci. Lett. 386, 149–160. https://doi.org/10.1016/j.epsl.2013.10.052.
- Lifton, N., Caffee, M., Finkel, R., Marrero, S., Nishiizumi, K., Phillips, F.M., Goehring, B., Gosse, J., Stone, J., Schaefer, J., Theriault, B., 2015. *In situ* cosmogenic nuclide production rate calibration for the CRONUS-Earth project from Lake Bonneville, Utah, shoreline features. Quat. Geochronol. 26, 56–69. https://doi.org/10.1016/j.quageo.2014.11.002.
- Lora, J.M., Mitchell, J.L., Risi, C., Tripati, A.E., 2017. North Pacific atmospheric rivers and their influence on western North America at the Last Glacial Maximum. Geophys. Res. Lett. 44, 1051–1059, 2016GL071541.
- Lora, J.M., 2018. Components and mechanisms of hydrologic cycle changes over North America at the Last Glacial Maximum. J. Clim. 31, 7035–7051. https://doi.org/ 10.1175/JCIJ-D-17-0544.1
- Lora, J.M., Ibarra, D.E., 2019. The North American hydrological cycle through the last deglaciation. Quat. Sci. Rev. 226 https://doi.org/10.1016/j.quascirev.2019.105991.
- Lora, J.M., Mitchell, J.L., Tripati, A.E., 2016. Abrupt reorganization of North Pacific and western North American climate during the last deglaciation. Geophys. Res. Lett. 43, 11796–11804. https://doi.org/10.1002/2016GL071244.
- Lorenz, D.J., Nieto-Lugilde, D., Blois, J.L., Fitzpatrick, M.C., Williams, J.W., 2016. Downscaled and debiased climate simulations for North America from 21,000 years ago to 2100AD. Sci. Data 3, 160048. https://doi.org/10.1038/sdata.2016.48.
- Marcott, S.A., Clark, P.U., Shakun, J.D., Brook, E.J., Davis, P.T., Caffee, M.W., 2019. ¹⁰Be age constraints on latest Pleistocene and Holocene cirque glaciation across the western United States. npj Clim. Atmosph. Sci. 2, 1–7. https://doi.org/10.1038/s41612-019-0062-z.
- Meierding, T.C., 1982. Late Pleistocene glacial equilibrium-line altitudes in the Colorado Front Range: a comparison of methods. Quat. Res. 18, 289–310.
- Menking, K.M., Anderson, R.Y., Shafike, N.G., Syed, K.H., Allen, B.D., 2004. Wetter or colder during the last glacial maximum? Revisiting the pluvial lake question in southwestern North America. Quat. Res. 62, 280–288. https://doi.org/10.1016/j. vares 2004.07.005
- Menking, K.M., Polyak, V.J., Anderson, R.Y., Asmerom, Y., 2018. Climate history of the southwestern United States based on Estancia Basin hydrologic variability from 69 to 10 ka. Quat. Sci. Rev. 200, 237–252. https://doi.org/10.1016/j. quascirev.2018.09.030.
- Meyer, G.A., Watt, P.M., Wilder, M., 2014. Was Mount Taylor glaciated in the Late Pleistocene? An analysis based on field evidence and regional equilibrium line altitudes. N. M. Geol. 36, 32–39.
- Morrill, C., Lowry, D.P., Hoell, A., 2018. Thermodynamic and dynamic causes of pluvial conditions during the Last Glacial Maximum in western North America. Geophys. Res. Lett. 45, 335–345. https://doi.org/10.1002/2017GL075807.
- Moench, R.H., Grambling, J.A., Robertson, J.M., 1988. Geologic map of the Pecos Wilderness, Santa Fe, San Miguel, Mora, Rio Arriba and Taos counties, New Mexico. US Geol. Surv. Miscellaneous Field Stud. Map MF-1921-B 1 (48), 000.

- Muzikar, P., Elmore, D., Granger, D.E., 2003. Accelerator mass spectrometry in geologic research. Geol. Soc. Am. Bull. 115, 643–654. https://doi.org/10.1130/0016-7606 (2003)115<0643:AMSIGR>2.0.CO;2.
- Nishiizumi, K., Imamura, M., Caffee, M.W., Southon, J.R., Finkel, R.C., McAninch, J., 2007. Absolute calibration of ¹⁰Be AMS standards. Nucl. Instrum. Methods Phys. Res. Sect. B Beam Interact. Mater. Atoms 258, 403–413. https://doi.org/10.1016/j. pipb.2007.01.207
- Oerlemans, J., 2001. Glaciers and Climate Change. Balkema Publishers, Lisse. xii, p. 148. Ohmura, A., Kasser, P., Funk, M., 1992. Climate at the equilibrium line of glaciers.

 J. Glaciol. 38, 397–411.
- Osman, M.B., Tierney, J.E., Zhu, J., Tardif, R., Hakim, G.J., King, J., Poulsen, C.J., 2021. Globally resolved surface temperatures since the Last Glacial Maximum. Nature 599, 239–244. https://doi.org/10.1038/s41586-021-03984-4.
- Oster, J.L., Ibarra, D.E., 2019. Glacial hydroclimate of western North America: insights from proxy-model comparison and implications for Lake Bonneville. In: Lund, W.R., McKean, A.P., Bowman, S.D. (Eds.), Proceedings Volume: 2018 Lake Bonneville Geologic Conference and Short Course, October 3-6, 2018, vol. 170. Utah Geological Survey Miscellaneous Publication.
- Oster, J.L., Ibarra, D.E., Winnick, M.J., Maher, K., 2015. Steering of westerly storms over western North America at the Last Glacial Maximum. Nat. Geosci. 8, 201–205. https://doi.org/10.1038/NGE02365.
- Oster, J.L., Weisman, I.E., Sharp, W.D., 2020. Multi-proxy stalagmite records from northern California reveal dynamic patterns of regional hydroclimate over the last glacial cycle. Quat. Sci. Rev. 241, 106411 https://doi.org/10.1016/j. dusciercy.2020.106411
- Palacios, D., Stokes, C.R., Phillips, F.M., Clague, J.J., Alcalá-Reygosa, J., Andrés, N., Angel, I., Blard, P.H., Briner, J.P., Hall, B.L., Dahms, D., Hein, A.S., Jomelli, V., Mark, B.G., Martini, M.A., Moreno, P., Riedel, J., Sagredo, E., Stansel, N.D., Vázquez-Salem, L., Vuille, M., Ward, D.J., 2020. The deglaciation of the Americas during the last glacial termination. Earth Sci. Rev. 203, 103113 https://doi.org/10.1016/j.earscirev.2020.103113.
- Pierce, K.L., 2003. Pleistocene glaciations of the Rocky Mountains. In: Gillespie, A.R., Porter, S.C., Atwater, B.F. (Eds.), The Quaternary Period in the United States. Developments in Quaternary Science 1. Elsevier, Amsterdam, pp. 63–76. https://doi. org/10.1016/S1571-0866(03)01004-2.
- Plummer, M.A., Phillips, F.M., 2003. A 2-D numerical model of snow/ice energy balance and ice flow for paleoclimatic interpretation of glacial geomorphic features. Quat. Sci. Rev. 22, 1389–1406. https://doi.org/10.1016/S0277-3791(03)00081-7.
- Polyak, V.J., Asmerom, Y., Burns, S.J., Lachniet, M.S., 2012. Climatic backdrop to the terminal Pleistocene extinction of North American mammals. Geology 40, 1023–1026. https://doi.org/10.1130/G33226.1.
- Porter, S.C., 1975. Equilibrium-line altitudes of late Quaternary glaciers in the Southern Alps, New Zealand. Quat. Res. 5, 27–47.
- Powers, W.E., 1939. Basin and shore features of the extinct Lake Saint Augustine, New Mexico. J. Geomorphol. 2. 345–356.
- Quirk, B.J., Moore, J.R., Laabs, B.J., Caffee, M.W., Plummer, M.A., 2018. Termination II, Last Glacial Maximum, and Lateglacial chronologies and paleoclimate from Big Cottonwood Canyon, Wasatch Mountains, Utah. Geol. Soc. Am. Bull. 130, 1889–1902. https://doi.org/10.1130/B31967.1.
- Quirk, B.J., Moore, J.R., Laabs, B.J., Plummer, M.A., Caffee, M.W., 2020. Latest Pleistocene glacial and climate history of the Wasatch Range, Utah. Quat. Sci. Rev. 238, 106313 https://doi.org/10.1016/j.quascirev.2020.106313, 1-17.
- Quirk, B.J., Huss, E., Laabs, B.J.C., Leonard, E., Licciardi, J., Plummer, M.A., Caffee, M. W., 2022. Late Pleistocene glacial chronologies and paleoclimate in the northern Rocky Mountains. Clim. Past 18, 293–312. https://doi.org/10.5194/cp-18-293-2022.
- Rasmussen, S.O., Andersen, K.K., Svensson, A.M., Steffensen, J.P., Vinther, B.M., Clausen, H.B., Siggaard-Andersen, M.-L., Johnsen, S.J., Larsen, L.B., Dahl-Jensen, D., Bigler, M., 2006. A new Greenland ice core chronology for the last glacial termination. J. Geophys. Res. 111, D06102 https://doi.org/10.1029/ 2005.JD006079
- Ray, L.L., 1940. Glacial chronology of the southern Rocky Mountains. Geol. Soc. Am. Bull. 51, 1851–1917.
- Refsnider, K.A., Laabs, B.J.C., Plummer, M.A., Mickelson, D.M., Singer, B.S., Caffee, M. W., 2008. Last Glacial Maximum climate inferences from cosmogenic dating and

- glacier modeling of the western Uinta ice field, Uinta Mountains, Utah. Quat. Res. 69, 130–144. https://doi.org/10.1016/j.yqres.2007.10.014.
- Refsnider, K.A., Brugger, K.A., Leonard, E.M., McCalpin, J.P., Armstrong, P.P., 2009. Last glacial maximum equilibrium-line altitude trends and precipitation patterns in the Sangre de Cristo Mountains, southern Colorado, USA. Boreas 38, 663–678. https:// doi.org/10.1111/j.1502-3885.2009.00097.x.
- Richmond, G.M., 1963. Correlation of Some Glacial Deposits in New Mexico. US Geological Survey Professional Paper 450, pp. E121–E125.
- Richmond, G.M., 1964. Glacial Deposits of Sierra Blanca Peak, New Mexico. New Mexico Geological Society 15th Field Conference, pp. 79–81.
- Schweinsberg, A.D., Briner, J.P., Shroba, R.R., Licciardi, J.M., Leonard, E.M., Brugger, K. A., Russell, C.M., 2016. Pinedale glacial history of the upper Arkansas River valley: new moraine chronologies, modeling results, and geologic mapping. In: Keller, S.M., Morgan, M.L. (Eds.), Unfolding the Geology of the West, vol. 44. Geological Society of America Field Guide, pp. 335–353. https://doi.org/10.1130/2016.0044(14).
- Schweinsberg, A.D., Briner, J.P., Licciardi, J.M., Shroba, R.R., Leonard, E.M., 2020. Cosmogenic ¹⁰Be exposure dating of Bull Lake and Pinedale glaciations and deglaciation in the upper Arkansas River valley, Colorado Rocky Mountains, U.S.A. Quat. Res. 97 https://doi.org/10.1017/qua.2020.21.
- Sharma, P., Bourgeois, M., Elmore, D., Granger, D., Lipschutz, M.E., Ma, X., Miller, T., Mueller, K., Rickey, F., Simms, P., Vogt, S., 2000. PRIME lab AMS performance, upgrades and research applications. Nucl. Instrum. Methods Phys. Res. Sect. B Beam Interact. Mater. Atoms 172, 112–123. https://doi.org/10.1016/S0168-583X(00) 00132-4
- Sheppard, P.R., Comrie, A.C., Packin, G.D., Angerbach, K., Hughes, M.K., 2002. The climate of the US Southwest. Clim. Res. 21, 219–238.
- Shroba, R.R., 1977. Soil Development in Quaternary Tills, Rock-Glacier Deposits, and Taluses, Southern and Central Rocky Mountains. PhD dissertation. University of Colorado, Boulder, p. 308.
- Smith, H.T.U., Ray, L.L., 1941. Southernmost glaciated peak in the United States. Science 93, 209.
- Stuiver, M., Reimer, P.J., Reimer, R.W., 2021. CALIB 8.2 [WWW program] at. http://calib.org. (Accessed 27 July 2021).
- Thompson, R.S., Whitlock, C., Bartlein, P.J., Harrison, S.P., Spaulding, W.G., Wright, H. E., Kutzbach, J.E., Webb, T.I.I.I., Ruddiman, W.F., Street-Perrott, F.A., 1993.
 Climatic changes in the western United States since 18,000 yr BP. In: Wright, H.E. (Ed.), Global Climates since the Last Glacial Maximum, pp. 468–513.
- Tripati, A.K., Sahany, S., Pittman, D., Eagle, R.A., Neelin, J.D., Mitchell, J.L., Beaufort, L., 2014. Modern and glacial tropical snowlines controlled by sea surface temperature and atmospheric mixing. Nat. Geosci. 7, 205–209. https://doi.org/10.1038/s41586-020-2617.
- Tulenko, J.P., Caffee, W., Schweinsberg, A.D., Briner, J.P., Leonard, E.M., 2020. Delayed and rapid deglaciation of alpine valleys in the Sawatch Range, southern Rocky Mountains, USA. Geochronology 2, 1–11. https://doi.org/10.5194/gchron-2-245-2020
- Van Devender, T.R., Betancourt, J.L., Wimberly, M., 1984. Biogeographic Implications of a Packrat Midden Sequence from the Sacramento Mountains, South-Central New Mexico 1, Ouat. Res. 22, 344–360.
- Ward, D.W., Anderson, R.S., Briner, J.P., Guido, Z.S., 2009. Numerical modeling of cosmogenic deglaciation records, Front Range and San Juan Mountains, Colorado. J. Geophys. Res.–Earth Surface 114, F01026. https://doi.org/10.1029/ 2008JF001057.
- Wesling, J.R., 1987. Glacial geology of Winsor Creek drainage basin, southern Sangre de Cristo Mountains, New Mexico. In: Menges, C., Enzel, Y., Harrison, B. (Eds.), Quaternary Tectonics, Landform Evolution, Soil Chronologies and Glacial Deposits—Northern Rio Grande Rift of New Mexico. Friends of the Pleistocene, Rocky Mountain Cell. Field Trip Guidebook, pp. 177–191.
- Wesling, J.R., 1988. Glacial Chronology and Soil Development in Winsor Creek Drainage Basin, Southernmost Sangre de Cristo Mountains, New Mexico. MS thesis, University of New Mexico, Albuquerque, p. 186.
- Wright Jr., H.E., Bent, A.M., Spross Hansen, B., Maher Jr., L.J., 1973. Present and past vegetation of the Chuska Mountains, northwestern New Mexico. Geol. Soc. Am. Bull. 84, 1155–1180.